UNIVERSIDAD TÉCNICA FEDERICO SANTA MARÍA

DEPARTMENT OF CHEMICAL AND ENVIRONMENTAL ENGINEERING

VALPARAISO, CHILE

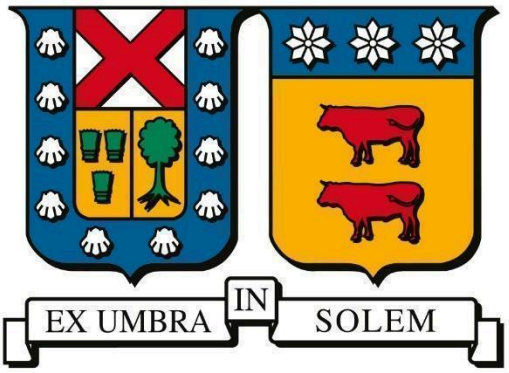

"Investigation of Carbon Produced by Pyrolysis: Characterisation and Processing"

Osamudiamen Emmanuel Agho

THESIS TO OBTAIN THE DEGREE OF MASTER OF SCIENCE IN CHEMICAL ENGINEERING

Main supervisor: Iván Cornejo García

Co-supervisor: Claudio Acuña Pérez

External supervisor: Julio Valenzuela

Joint Master Erasmus Mundus

June 2024

VALIDATION AND CONFIDENTIALITY RECORD FOR
THESIS IN THE ACADEMIC REPOSITORY

1.- IDENTIFICATION OF THE ACADEMIC WORK

Type of monograph (check one): ☐ Thesis / Final Project ☒ Thesis (Master/PhD)

Title of the work: Investigation of Carbon Produced by Pyrolysis: Characterisation and Processing

Candidate's name: OSAMUDIAMEN EMMANUEL AGHO

Program / Degree: Magister en Ciencias de la Ingeniería Química

Campus: Casa Central Valparaíso **Department:** Ingeniería Química y Ambiental

2.- VALIDATION BY THE ADVISOR / THESIS DIRECTOR

I, IVÁN ANDRES CORNEJO GARCÍA, in my capacity as Advisor/Director of the academic work mentioned above, hereby **CERTIFY** that:

- I have reviewed this document, and it corresponds to the final approved version of the work.
- The work meets the academic and formatting requirements established by the institution.

3.- CONFIDENTIALITY EVALUATION FOR INDUSTRIAL PROPERTY (check one)

☒ The work DOES NOT contain information that warrants confidentiality and may be published immediately in the open-access repository.

☐ The work CONTAINS information with potential industrial or intellectual property implications and requires a confidentiality period (**embargo**) for (check one):

☐ 6 months ☐ 12 months ☐ 2 years ☐ 3 years ☐ 5 years ☐ 10 years

Justification for the need for confidentiality (mandatory if an embargo is requested):

4.- SIGNATURES

Advisor or Director of the project/thesis:

Date: 24/04/2026 **Signature:** 

Student or Candidate:

Date: 24/04/2026 **Signature:** 

FACULTY OF TECHNOLOGY, OULU MINING SCHOOL, UO

DEPARTMENT OF MINERAL RESOURCES ENGINEERING, MUL

FACULTY OF MINING, GEOLOGY AND PETROLEUM ENGINEERING, UNIZG

DEPARTMENT OF CHEMICAL AND ENVIRONMENTAL ENGINEERING, USM

Investigation of Carbon Produced by Pyrolysis: Characterisation and Processing

Osamudiamen Emmanuel Agho

DEGREE PROGRAMME EMJM-PROMISE

Erasmus Mundus Joint Master in Sustainable Mineral and Metal Processing Engineering

June 2024

Chair of Mineral Processing
Montan Universität, Leoben

Investigation of Carbon Produced by Pyrolysis: Characterisation and ProcessingS

Agho, Osamudiamen Emmanuel

SUSTAINABLE MINERAL AND METAL PROCESSING ENGINEERING
Master's thesis

June, 2024

Acknowledgment

First and foremost, I wish to express my sincere appreciation to almighty God for his grace in seeing me through to the end of my master's programme.

My gratitude also goes to my wife and son for being my support system throughout my programme.

Also, many thanks to my family members for their encouragement and well wishes.

I will not forget the efforts of my supervisors, Univ.-Prof. DI Dr. mont Flachberger Helmut and DI Hartig Gerald, for their mentorship and in-depth supervision, respectively.

I will not fail to recognise the EMJMD-PROMISE consortium, where it all began, and all my lecturers in the consortium.

Lastly, my thanks go to members of my class for their input and motivation in one way or another. The journey wouldn't have been complete without them.

Abstract

The generation of pyrolytic carbons through pyrolysis is rising due to energy recovery in the form of pyrolysis gas and pyrolysis oil from various waste sources, as well as the production of hydrogen from methane decomposition. In parallel, the demand for many forms of carbon is on the rise. Therefore, to make pyrolytic carbon viable for applications, further processing steps are necessary

In this thesis, pyrolytic carbons derived from the pyrolysis of polyolefin (PyCP) and methane gas (CMP) were investigated. Separation methods such as flotation, settling velocity, and wet magnetic separation were used for the purification of PyCP. Reverse flotation of PyCP showed some promising results for carbon grade improvement. CMP is considered the purest and finest of all pyrolytic carbon samples received. Agglomeration tests were performed on CMP to improve its transportability and applicability. Lignosulfonate binders were considered the best based on high compressive strength test results in comparison with other binders.

There are many potential applications for the purified carbons of the PyCP, such as improving the carbon surfaces.

Table of Contents

Chapter 1: Introduction and Background of Study

The concept of energy recovery and decarbonisation will always be in the scope of all modern processes to tackle the dual challenge of energy efficiency and global warming [1].

Energy recovery from hydrocarbon often refers to procedures that extract or harness energy from carbon-containing molecules or materials [2]. There are several methods for energy recovery from hydrocarbon waste with waste-to-energy (incineration) and pyrolysis being the principal ones [1].

Regardless of the process for energy recovery used, the goal often remains the same: maximising energy generation through waste reduction, applications of side streams, and products for other energy utilisation processes [6]. Alongside most energy recovery processes and any industrial process is the control of emissions or possible ways of eliminating them due to the impact of global warming [7].

Similarly, the processes of decarbonisation and energy utilisation can often result in solid carbons of interest with varied applications, especially from modern thermal waste to energy processes such as pyrolysis [3][4].

1.1. Pyrolysis

Pyrolysis is a process that incorporates the heating of organic materials in the absence of oxygen, generally, to produce carbon-rich products (char), oils, and pyrolysis gas [12].

However, the type of product is often dependent on the type of material used for the pyrolysis process [13]. Regardless, it is an important method used to produce carbon with diverse applications across different industries [6]. Many publications on pyrolysis are easily found in the literature [3][4][5].

Another carbon of interest is that generated from the pyrolysis of methane for the generation of hydrogen gas used for the decarbonisation of industries. Regardless of whatever organic source is used for the pyrolysis, the process is always a decomposition of the original feed material.

1.1.1. Types of Pyrolysis

There are types of pyrolysis classified as:

1. Carbonisation is often regarded as the complete pyrolysis of organic matter into solid carbon, known as charcoal. It can be scientifically described as the gradual progress of a carbon compound under the influence of rising temperatures, resulting in the loss of liquids and gases, and leaving behind a solid product [8].
2. Slow pyrolysis: this is otherwise regarded as low-temperature pyrolysis, typically below 400°C [9].
3. Medium temperature pyrolysis occurs at temperatures between 400 and 600°C [9].
4. Fast pyrolysis: this type occurs at temperatures above 600°C and is often used to produce bio-oils [10].

1.1.2. Reactor Types Used in Pyrolysis.

The reactor types often used for most pyrolytic processes include cyclone reactors, rotating cone reactors, circulating fluidized bed reactors, vacuum pyrolysis reactors, and microwave or molten salt reactors [11].

These reactors can also be classified based on their energy transfer methods. e.g., microwave and plasma, the reactor designs, e.g., a fluidized bed, a bubble column, or a combination of two or more technologies, e.g., moving bed reactors [11].

A look into energy recovery and decarbonisation through pyrolysis is very promising when compared to other processes. Also important is the abundance of materials necessary for the process. A typical example of such materials would be polyolefins, an abundant municipal solid waste (MSW). Methane gas, a naturally abundant, cheap gas that can also be obtained from biodegradables, can also be considered.

1.2. Statement of Task

The generation of pyrolytic carbons through pyrolysis is rising due to energy recovery in the form of synthetic gas, pyrolytic oil, hydrogen gas from methane, waste plastics from MSW, etc. Also, the demand for these carbons is on the rise but not without adequate purification and processing to an acceptable state.

This thesis will deal with the possible purification and agglomeration of some pyrolytic carbons of interest.

1.3. Aim and Objective

The general scope of this work is about the characterization, purification, and agglomeration of pyrolytic carbons from polyolefins (PyCP) and carbon from methane plasmalysis (CMP).

The specific objectives are:

1. Optimisation of flotation of grade-recovery of processed graphite using different reagent concentrations and volume percent of solid content in a Denver and pneumatic flotation cell.
2. To check the feasibility of separation and grade improvement of PyCP using flotation, magnetic, and settling velocity methods
3. To test for influence of water content and different binders on the compressive strength of the CMP from plasma pyrolysis of methane gas through pressure and tumble growth agglomeration.

Based on objective 1 above, the feasibility of using graphite flotation as a model for the flotation purification process of PyCP was studied. Also, the agglomeration test results will provide the needed information for a data handling sheet for transportation and storage purposes.

Chapter 2: Literature Study

The literature study looked at the techniques used for the beneficiation of graphite, a natural carbon, the description and characteristics of polyolefins, the pyrolysis reactions, the pretreatment process, and applications of PyCP. Furthermore, a look at the hydrogen economy and the modern trend towards hydrogen production from methane pyrolysis, along with a description of the various CMPs from it, were reviewed. Lastly, the general agglomeration process and compressive strength method of testing were also looked at.

3.1. Review of Techniques used for Graphite Beneficiation

Graphite is one of the most prevalent naturally occurring polymorphs of crystalline carbon, along with diamond. The creation of graphite is a result of contact or regional metamorphism of sedimentary organic matter [16]. Among its several applications is the production of graphene, which is a highly conductive material used in batteries for green energy transition [17].

Like most minerals, the size of graphite is reduced through comminution for liberation. Liberated graphite is inherently hydrophobic and floatable, and it is generally established that liberation has a key effect on increasing recovery and grade [18]. The type of comminution method used varies with the graphite type. However, the main goal is to prevent very fine graphite particles [18]. Flotation is the principal beneficiation process for graphite since the mineral is highly hydrophobic. However, despite its natural flotability, the separation from gangue minerals is often dependent on the addition of surfactants and depressants [19].

With regards to the flotation process itself, several works have been attributed to fine particle flotation, of which graphite is considered a part because of its median size fractions of 20.5µm of some processed products [24]. In general, the flotation performance of particles between 20 and 150µm is often considered true flotation because there is little effect due to entrainment [22][23].

Conversely, particles of size class <20µm are poorly recovered by flotation due to a decreased particle-bubble collision probability [25]. Because tiny particles are easily deflected by their low mass (and inertial force), they are deflected by hydraulic drag forces caused by miniature whirlpools in a turbulent environment (mechanical flotation reactors) and rising bubble swarms

(pneumatic flotation reactors). As a result, small particles tend to follow the fluid streamlines around the bubbles rather than collide with them [25][26].

A comprehensive review of the various adaptations used for the flotation of fine particles is carried out by Tattu et al [27]. However, a more recent novel approach in reducing bubble size for improved energy of collision [29]and the use of hydrophobized glass bubbles for improving grade recovery has been done [28].

The production of a higher purity of graphite is also done by the acid leaching technique, often done after flotation with the use of common inorganic acids [21]. Leaching reduces impurities and can also be done before flotation to remove gangue [20]. This combination of flotation and acid leaching has been shown to be effective for the purification of graphite [21].

3.2. Pyrolytic Polyolefins

The disposal of MSW organic and plastic waste takes different forms based on technology and interest. One of the possible ways of disposing of such waste is through the valorisation of this waste by pyrolysis. As an important process used for the production of carbon with diverse applications for different industries [14], it has come to the fore in most research work.

One of the materials of interest for this work is polyolefins, polymers of alkenes often known as polyethylene and polypropylene.

Table 1 below shows some of the properties of this polymer.

Table 1: Properties of Polyethylene [42]

Properties of Polyethylene	
Density	0.910-0.965 g/cm^3
Crystallinity	From low crystalline and high amorphous to high crystalline to low amorphous
Characteristics	Flexible and good transparency Good moisture barrier properties High impact strength at low temperature

The pyrolysis of this type of material is of importance to modern society, considering the volume of plastic waste generated globally for the year 2019 as 353 million tonnes and 53.1 million tonnes in the EU alone [15].

3.2.1 Pyrolysis of Polyolefins

Generally, pyrolysis is often applied for the recycling of polymeric waste for the production of chemicals as feedstock [1][2] and carbonaceous materials [3]. For these processes, the use of catalysts is essentially considered a primary factor [31][32][33]. However, most techniques using catalysts for polyolefin cracking have the disadvantage of requiring significant concentrations of catalysts up to 20 wt% in relation to the polymer feedstock [34]. Recent experiments, however, showed the use of Lewis acids like $AlCl_3$ and mixtures with $TiCl_4$ to increase the contact of the polymer melt with the catalyst [34].

A comparative study on the pyrolysis of polyolefins and polyethylene terephthalate (PET) leads to the formation of tar with mainly paraffinic and aromatic structures, respectively [35]. On the other end, the production of wax from polyolefins is subjected to a temperature of 450–600°C in a conical spouted bed reactor [36].

The production of useful carbon for reinforcement was by the production of carbon nanotubes (CNT) through the passage of gaseous products from the pyrolysis of polyolefins and other plastics through a chemical vapour deposition reactor at 700°C, and product enhancement was by the use of Fe and Co catalysts [37]. Also, CNT can be produced from pyrolysis oil [38] and hydrogen production [39].

Furthermore, it is an innovative process for the production of multi-wall carbon nanotubes by the pyrolysis of virgin or recycled polyolefins [41]. However, further investigations are needed to determine the product quality. The few works on pyrolytic carbon from olefins show the possibility of generating CNT. However, the issues of purity and improvement of carbon quality are yet to be analysed.

Pyrolytic carbons are generally similar to graphite but with some covalent bonding as a result of imperfections [40]. They are also considered to have a high strength-to-weight ratio with unique thermal properties and diamagnetic properties against the cleavage plane at room temperature [40]. However, these similarities cannot be clearly distinguished due to the anisotropic nature of carbon itself.

3.2.2. Treatment Processes of Pyrolytic Carbons from Polyolefins

As already mentioned, the pyrolysis process converts the plastic waste into useful materials and fuels at the required temperature and in the absence of oxygen. One of such material produced is the PyCP of interest.

The properties of PyCP are determined by the kind of plastic, the presence of a catalyst, and the reaction parameters, such as temperature, residence time, and pressure [64]. Also, is the use of catalyst like acidic zeolites during pyrolysis for the production of aromatic and polycyclic aromatic hydrocarbons [66].

Polyolefins waste can undergo pretreatment processes such as screening, sorting, washing and flotation to improve the quality of the products from pyrolysis. These pretreatment processes act as first step purification stage and the removals of metals can be by magnetic, electrostatic and eddy current [67]. The use of flotation method as part of the pretreatment process for the removal of non-polyolefin polymers such polyvinylchloride and PET is not only dependent on the hydrophobicity but also on the size, density, and shape of the particles [68]

At the time this thesis was written, there was no work in literature about the purification of the PyCP, however, a similar work by Niu Xiaolu [69] on an invention of pyrolytic carbon black purification of waste tires through a series of acid and alkali washing steps followed by a combined acid-alkali washing process reduced the ash and volatile components.

These PyCPs play an important role in the circular economy by turning plastic waste into useful resources, increasing sustainability and resource efficiency. They can be utilised to produce graphene, nano-catalysts, adsorbent materials, nano-fillers for composite applications, sensors, and supercapacitors [65]. The possible applications of PyCPs are numerous and ongoing, with the goal of discovering sustainable and effective ways to recycle plastic waste and reduce dependency on non-renewable resources.

3.3. Methane Pyrolysis and Hydrogen Economy

The global dependence on fossil fuels for all human activities remains unchanged [43], despite the huge investment in clean energy. This, of course, has led to a high rise in CO_2 emissions

and global warming. The hydrogen economy entails the production, delivery, and use of hydrogen as a renewable energy source to decarbonise many sectors, such as heavy manufacturing, long-haul transportation, and electricity generation. In pursuit of this type of economy, several methods of hydrogen production are available, such as Steam Methane Reforming (SMR), electrolysis, biological methods, and other methods like solar water splitting, methane pyrolysis, and biomass gasification [44]. However, the degree of emissions varies with each process, a characterisation known as the colours of hydrogen [45].

A particular production process of interest is the thermal decomposition of methane gas (TDM), also known as methane pyrolysis. The main advantage of TDM over others is that it produces hydrogen gas and solid carbon. The global reaction equation is:

$$CH4_{(g)} \rightarrow C_{(s)} + 2H_{2(g)} \qquad \Delta H_r{}^{o} = +75KJ/mol \qquad \text{equation (1)}$$

This reaction can be with or without a catalyst, resulting in a lower or higher reaction temperature, respectively. Due to these conditions (cost of catalyst and high reaction temperature), the profitability of this process is lower when compared to other traditional hydrogen production processes like SMR. Therefore, finding suitable applications for the solid carbon can help boost the profitability of this process [46].

3.3.1 Pyrolytic Carbon types from Thermal Decomposition of Methane

Several carbon products, such as graphite-like carbon, carbon black, amorphous turbostratic carbon, filamentous carbon, and nanotubes, have been reported [46]. These carbon products are, however, dependent on the availability of catalysts (with or without), catalyst type, and reaction temperature. This is shown in Figure 1 below.

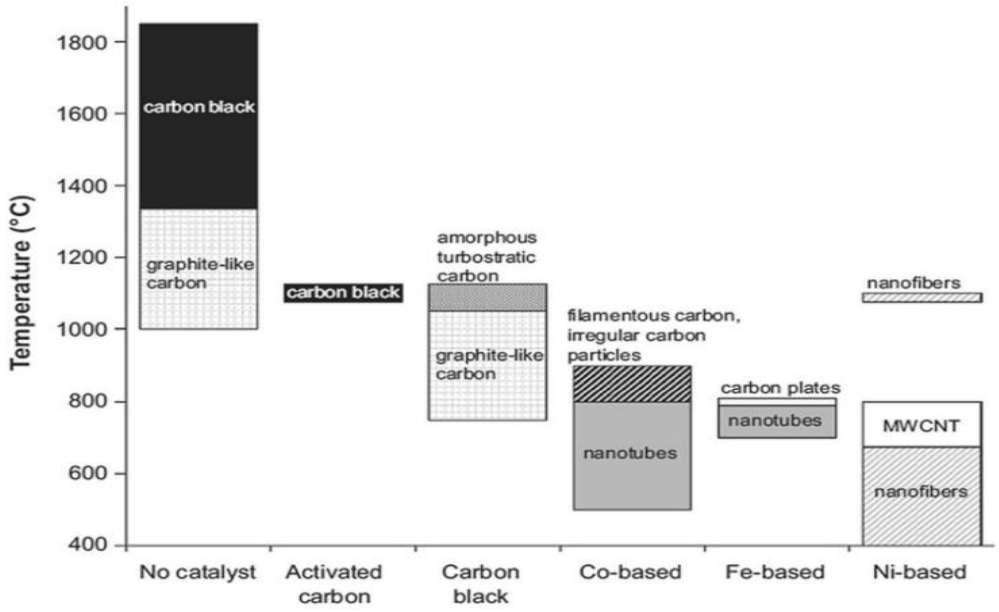

Figure 1. The TDM carbon type and dependence on temperature and catalyst types [46]

The varied applications of these carbon types can be summarised in Figure 2 below.

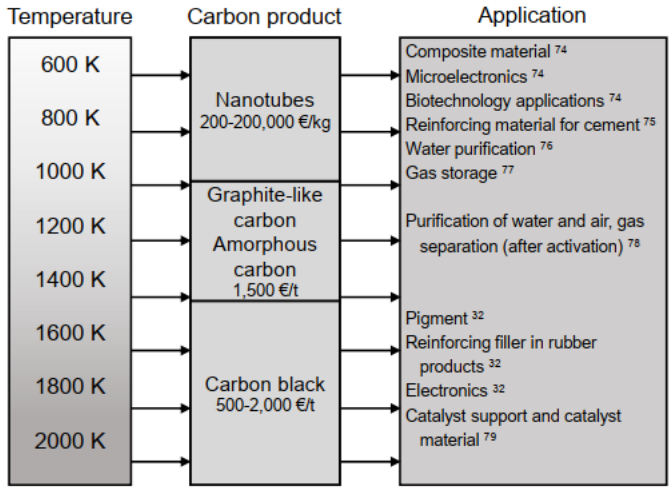

Figure 2. Dependency of carbon types on temperature and applications [47][48].

The TDM resulting in carbon black is always at a high temperature >1500, as shown in Figure 1. However, the thermal catalytic decomposition results in other variants of carbon. The major drawback is that the catalyst is often deactivated due to carbon deposition on the active sites and pores [50].

In recent times, the use of molten metal reactors has been used to address the issue of catalyst deactivation, thus eliminating the frequent need for catalyst regeneration [51]. This has,

however, led to the challenges of carbon contamination from the metallic elements in direct contact with them [78]. Thus, the focus is on further processing of the carbon for contamination removal. This is absolutely important because the profitability of methane pyrolysis is dependent on the solid carbon advantages of its applications, as mentioned. Also, the potential of these carbons is very high and can range from 280€/ton to 310€/ton, depending on the carbon product and purity [49].

Hartig G., Gehringer S., and Flachberger H. [52] carried out a one-stage test for the enrichment of carbon preconcentrate from methane pyrolysis using a tribo-electrostatic belt separator.

3.3.2 Agglomeration

A possible application of CMP is in agriculture for soil enrichment (as a substitute for biochar) [46][60]. Due to its fineness and bulk density, effective handling is of great importance and a major way of doing this is by agglomeration.

Agglomeration is the process of mixing smaller particles to form larger ones. Carbon black agglomeration can occur through several techniques, such as combining with liquids, exerting pressure, or heating [53]. The general methods of agglomeration are tumble or growth (pellets), pressure, and agglomeration by heat or sintering [54].

It is primarily aimed at reducing dustiness and other improved handling conditions such as low bulk density, segregation, and difficult flow [55].

The basic mechanisms of growth agglomeration have been classified as nucleation, coalescence, growth, and layering as shown in Figure 3. Forces contributing to the formation of pellets can be classified as natural or applied (mechanical), where natural forces are mainly due to Van der Wall's or electrostatic forces or interlocking effects of the particles [56][57].

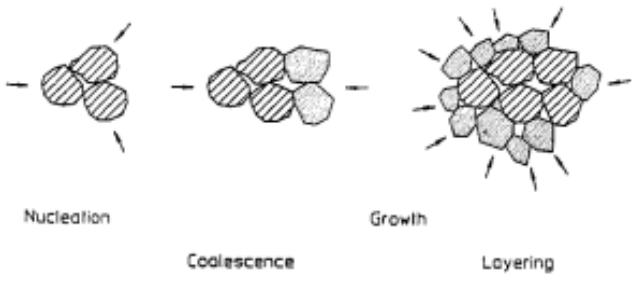

Figure 3. Basic mechanism of tumble growth agglomeration [54]

Pressure agglomeration, unlike tumble/growth agglomeration, is utilised to achieve one or more, and sometimes all, of the process conditions and product properties [54]. The structural change in bulk mass due to the application of external force is varied, and the determination of stress is also a major consideration for pressure agglomeration.

Salas-Bringas et al did a comparison between the uniaxial and diametral compressive tests and concluded that the average strength obtained in the diametral test is a better representation of the material strength due to the lower variance [57].

When evaluating material strength, it is important to be able to measure it regardless of the specimen's shape or size. However, this is often difficult to achieve. It is then more reliable to quantify strength using the area of the applied stresses.

Chapter 3: Sample Description

A description of the samples and their sources are as follows:

3.1. Graphite

The processed graphite was provided by the Chair of Mineral Processing at Montanuniversität Leoben with 40 wt% water and a particle density of 2.32 g/cm^3. Processed graphite was prepared for different vol.% of graphite, and flotation tests were carried out.

The samples for the Denver and pneumatic flotation were tagged as GFLOT 1, 2, and 3 (for 5, 2.5, and 7.5 vol% of graphite) and PG FLOT (2.5 vol% of graphite), respectively.

3.2. Pyrolytic Carbon from Polyolefin

Two separate bulk samples of PyCPs (I and II) were provided, feed for pyrolysis had at least 90 wt% polyolefines, which were completely pyrolyzed, were used as received. Both samples were provided by NGE (https://nge.at/en/), and PyCP I and II were of different heating temperatures in the pyrolysis process. The densities for both loose and compact are 898.7 g/L and 976 g/L, respectively. Particle density using a Micromeritics AccuPyc-1340 gas pycnometer was measured as 1.76 g/cm^3. A qualitative overview of both samples indicated that PyCP I contains some residual oil from pyrolysis with a coarser particle size distribution, while PyCP II has negligible oil and is much finer. Figure 4 shows the pyrolyzed and unpyrolysed PyCP.

With a specific surface area of 31.06 m^2/g, there is the likelihood of functionalization for other purposes based on the surface area (porosity) [62]. Elemental sample description of the bulk is shown in Table 2 below.

Table 2. Elemental composition from a handheld XRF using Geochem calibration.

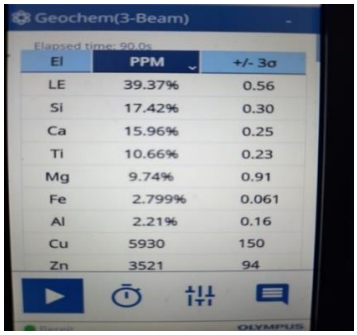

Figure 4. (a) 90wt% unpyrolyzed polyolefins (b) Pyrolyzed polyolefins

Generally, the starting material influences greatly the description of the PyCP [58]. However, majority of other pyrolytic reactions are often left with carbon with considerable amounts of impurities [59].

3.3. Carbon from Methane Plamalysis

CMP containing almost 100 wt% carbon and specific surface area of 22.76 m^2/g were utilised as received from an industrial plasmalyzer (plasma pyrolysis of methane) was mixed with different binders of lignosulfonate, corn starch, clay, and water to test for compressive strength upon granulation due to intensive mixing and the distribution of the materials for each of the binders.

Chapter 4: Experimental

This chapter will delve into the methodology, equipment, and reagents used for experimental tests, the experimental execution of each test done, and the analysis of the results obtained. A general characterization of all samples was done by sieve analysis and surface area, while image analysis was for PyCP. Purification of PyCP and graphite was done using flotation and settling velocity experiments, and handling was improved by agglomerating CMP. The Loss on Ignition (LOI) was also carried out to determine the carbon content of samples after purification.

4.1. Equipment and Reagents

4.1.1. Denver Cell

A Denver cell of volume 1280ml was used for flotation with an impeller speed of 1000rpm and air flow rate kept constant at 4 L/min Figure 5. Reagent used are as shown in Table 3

Table 3. Reagent types used for flotation.

Reagents	Description	mass(g)/drop
Montanol 800	Frother &Collector	0.018
Methyl Isobutyl Carbinol (MIBC)	Frother	0.016
Ekofol 452	Frother & collector	0.009
Diesel	Collector	0.01281

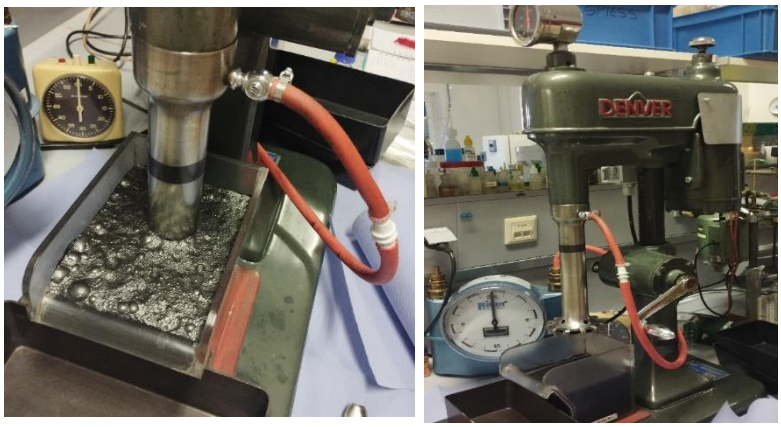

Figure 5. (a) denver cell during flotation (b) before flotation

4.1.2. Pneumatic Cell

An allmineral pneumatic flotation cell allflot® AF02 with a separate condition unit, 50L volume, air pressure of 3 bar, air flow between 20 and 40 L/hr and a pump speed of 7L/min was used to collect each froth product Figure 6. Ekofol 452 was the only reagent used for this cell.

Figure 6. Allmineral pneumatic cell with separate conditioning unit.

4.1.3. Settling column

A settling column of height 1.05m and diameter 0.15m for varied flow rates based on the desired settling velocity for particular size of interest. Settling time used for all test was 15min.

4.1.4. Magnetic Separator

A GMW model 347 dipole electromagnet with an external stirrer, ampere generator and a steel ball matrix was used for wet magnetic separation. Magnetic separation is performed using a wet high intensity magnetic separation mechanism. The magnetic property of products and residue is compared based on that of magnetite by using a Satmagan Figure 7.

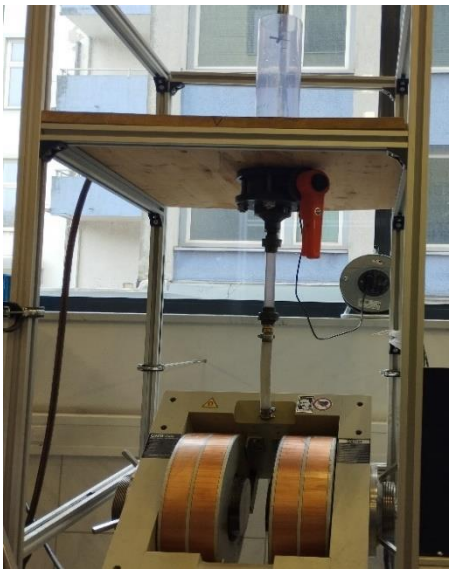

Figure 7. (a) GMW model 3473 dipole electromagnets (b) Satmagan

4.1.5. Mixer Granulator

Granulation was performed using an Eirich mixer-granulator with varying rotational speeds for granulation, as shown in Figure 8.

Figure 8. Eirich mixer-granulator

4.1.6. Pressure Agglomerator

Cylindrical pellets by cold pressing using a Messphysik MIDI 10 material testing press Figure 9. The surface diameter disks are 15cm. A set point for speed of compaction is set and all readings are from a computer connected to the press.

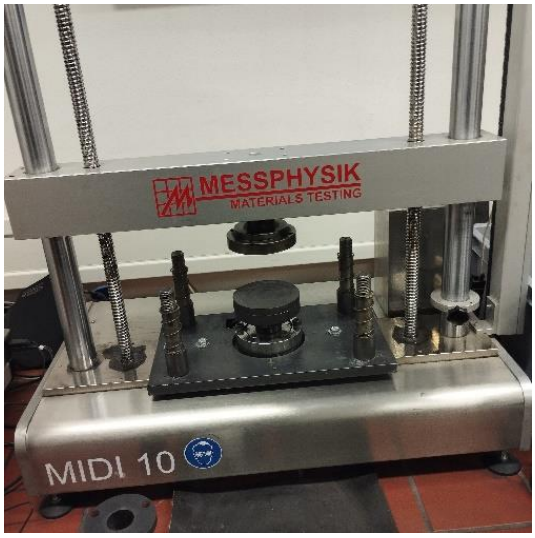

Figure 9. Messphysik MIDI 10 material testing analytical press

4.2. Methodology

The general methodology used for the experiments are:

4.2.1. LOI of Fixed Carbon

LOI is a widely used method to measure the amount of organic matter and carbonate mineral content (and indirectly for organic and inorganic carbon) [61]. Two split samples of mass 0.4–0.6g was weighed in clean crucibles and placed inside a Nabartherm muffle furnace, Figure 10, where a 1000 °C temperature was attained and held for 1 hour before cooling down. The weight of each sample after heating was recorded to determine the mass of carbon bunt off as volatiles.

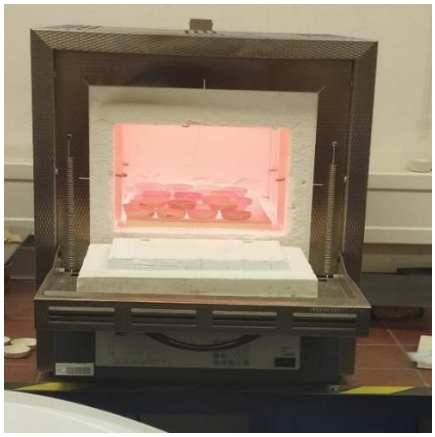

Figure 10. Nabartherm muffle furnace for burning off combustible

4.2.2. Image Analysis of PyCP

Polished sections for microscopic image analysis of two class size of the bulk sample I (100-500µm and <100µm) were done using a Buehler Metaserv 250 grinder polisher Figure 11. The polished sections were then viewed in three dimensional and point- surface perspective using a Leica M165 C stereo 3D and Leica MC170 HD respectively. Figure 12 shows the microscopes used.

Figure 11. Buehler Metaserv 250 grinder polisher

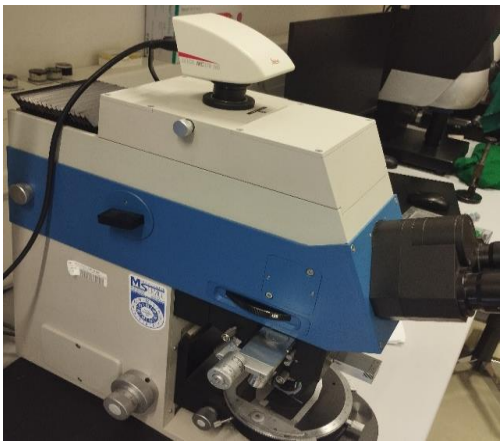

Figure 12. (a) Leica M165 C stereo (b) Leica MC170 HD

4.2.3. Particle Size Distribution - PSD

Sample splitting of bulk materials was by a sample splitter and sieve analysis is done by hand for larger size classes while fines < 100µm were done using a Malvern Mastersizer 3000 shown in Figure 13.

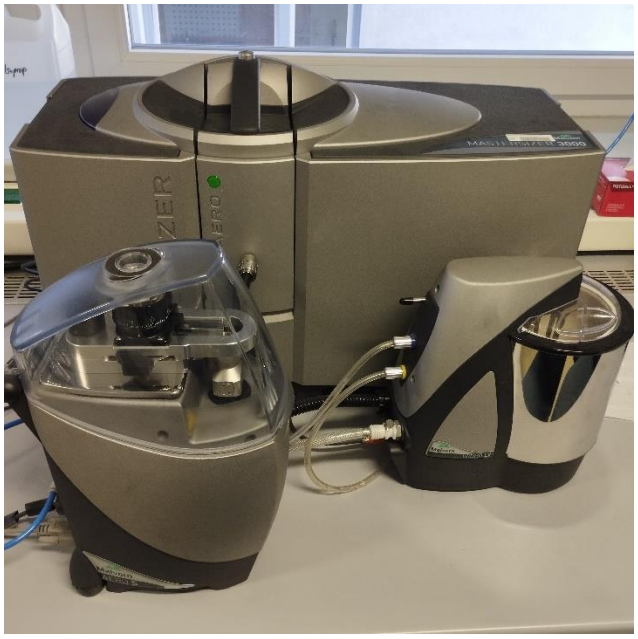

Figure 13. Malvern Mastersizer 3000 for particle size classification

Samples of interest were placed in a chamber, where they were fed into the equipment by vacuum suction. Three runs are done, and the individual and average size distributions are generated. This process is repeated until multiple measurements in a row show compatible results.

4.2.4. Surface Area

The surface area was determined using a Micrometric Flowsorb 2300 Brunauer–Emmett–Teller (BET) analyser with nitrogen as the analysing gas Figure 14. The operating pressure and temperature of the equipment is 957mbar and 22 °C with temperature regulation using liquid nitrogen. Three trials were conducted, and an average taken.

Figure 14. Micrometric flowsorb BET analyser.

4.3. Graphite Recovery

4.3.1. Goal

The recovery of processed graphite from contaminants by evaluating the effect of process parameters such as volume concentration, reagent types used and dosage for flotation test.

4.3.2. Execution

An initial test for the best volume percent and reagent was done using the Denver cell. A further flotation test was done for the best volume percent and reagent using a pneumatic cell.

4.3.2.1. Graphite Flotation test – Denver Cell

An initial trial for different reagent in Table 3 above and a 5v% (GFLOT1) was carried out to determine the best reagent to be used. Ekofol 452 was selected as the best reagent.

Optimal volume percent test with varying ekofol regime was conducted for 2.5, 5 and 7.5 v% (GFLOT1 to 3) of graphite by weighing 123.7g, 247.5g and 346.5g (74.24, 148.48, and 222.72g on dry basis), respectively, of the graphite sample and volume of the cell attained by filling it with water for each corresponding volume percent.

The mixture is stirred and conditioned with the reagent of interest. Table 4 below gives the description of the reagent dosage for each sample.

Table 4. Denver flotation using ekofol 452 for varying volume concentrations.

Sample	V% graphite	Reagent dosage(drops)	Total reagent(g)/tonfeed
GFLOT1	5	6-4-4	894.63
GFLOT2	2.5	3-5-7	1880.75
GFLOT3	7.5	5-4-7	723.04
GFLOT3 Error.	7.5		587.05

Ekofol 5drops + Montanol 4drops

The conditioning time for all samples was fixed at 2 minutes; the interval between each froth product was 28, 19, and 11 minutes; and a total time of 60 minutes was used for each flotation.

Each flotation product was dried for 24 hours at 105°C and weighed. This is to ensure that there is no water left, as the moisture effect can influence the prediction of carbon content from loss on ignition analysis.

4.3.2.2. Graphite Flotation test – Pneumatic Cell

A 2.5 v% was only considered for the pneumatic flotation test because it gave the best result from the Denver cell. This volume percent of graphite was by the addition of 46.82 litres to 4.833kg of graphite (dry mass = 2900g). The reagent regime is based on the same ratio as that of GFLOT2 (2.5 v%) in the Denver cell. Initial 117 drops (1.053g) of ekofol were added, and conditioning was simultaneously done in the tank, which is separated from the cell.

The second dosage was an addition of 195 drops (1.755 g), and five products with a 7-minute interval were collected. Collection was enhanced by the lifting of the plunger to depress the cone, which reduces froth height at regular intervals in the later froth products.

This was also repeated for the third-stage flotation with six froth products and the addition of 273 drops (2.457g).

A separate flotation of the initial residue was further done to see the percentage recovery, if any. This was carried out by repeating the same amount of reagent used for the last froth product (273 drops, 2.457 g).

The total time used for the entire test was 105 minutes. Drying was done for 24hrs at 105 °C and LOI carried out for dried products.

4.3.3. Results and Discussion - Graphite Flotation

4.3.3.1. Denver Cell

Description of reagent used and dosage are shown in Table 5 for the selection of the best reagent.

Table 5. Reagents descriptions used for initial Denver cell flotation of graphite.

Sample	Description	Total reagent(g)/tonfeed
GFLOT1A	14 drops ekofol once	878.78
GFLOT1B	10 +4 drops ekofol	866.75
GFLOTM	Montanol 3/2/2	876.77
GFLOTDM	MIBC4/4/2 + Diesel4/3/3	**1958.00**
	MIBC	1087.4
	DIESEL	870.6

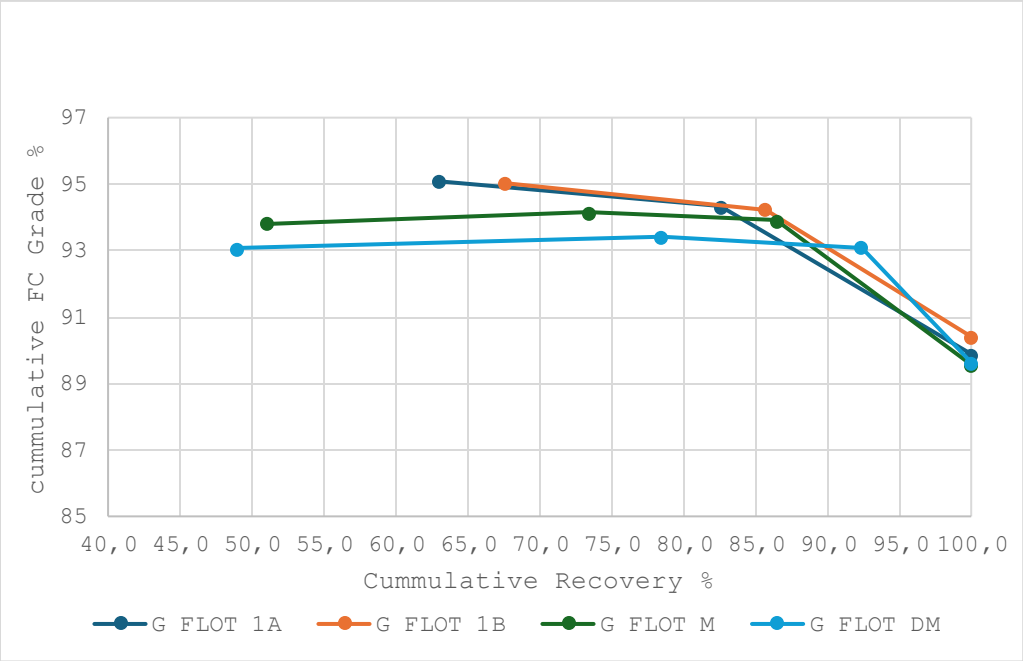

Figure 15. Grade-recovery for different reagents and regime of GFLOT1.

From Figure 15 above, the best grade recovery was between GFLOT 1A and GFLOT 1B, with GFLOT 1B giving a better recovery than GFLOT 1A. The tables of flotation product grade and recovery for the different reagents are shown in Appendix 1. The selected reagent and slightly

modified regime used for GFLOT 1B were used for the Denver cell flotation with different volume percents as shown in Figure 16 with GFLOT 2 (2.5 vol%) having better grade when compared to other volume percents used.

Tables of the grade and recovery for the different volume percent using ekofol 452 reagent samples of the Denver flotation are shown in Appendix 2.

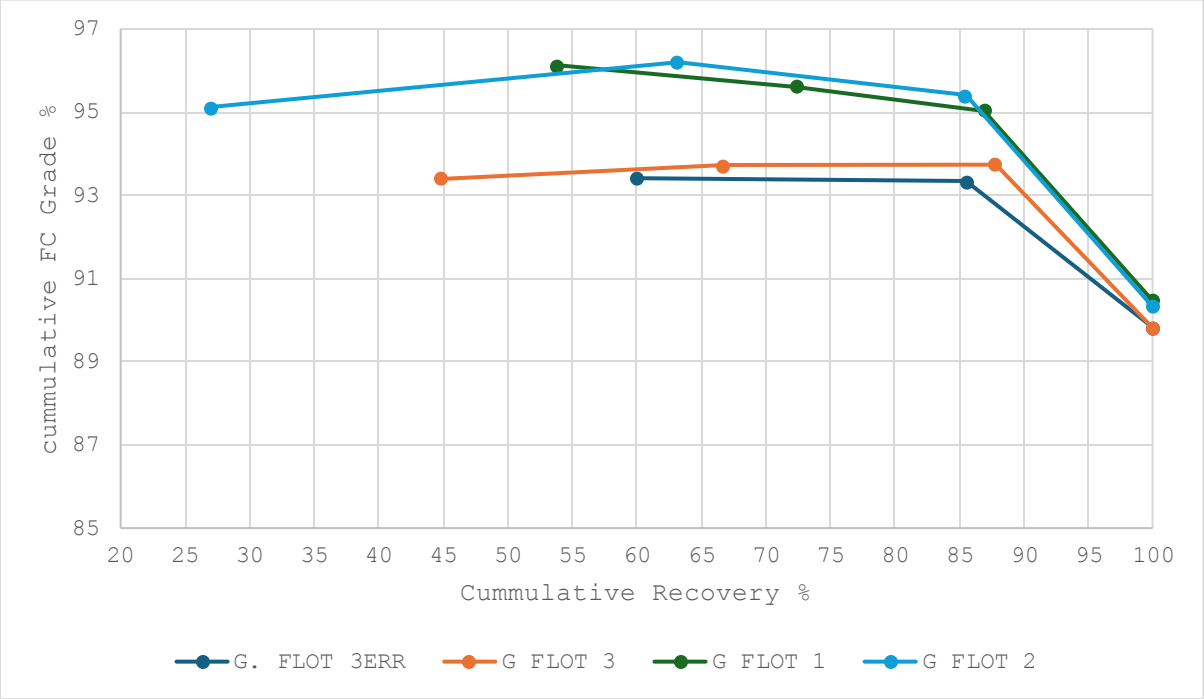

Figure 16. Different volume percent of graphite using Ekofol 452 as reagent.

4.3.3.2. Pneumatic Cell

Based on GLOT 2 (2.5 vol%) and ekofol 452 as volume percent and reagent of choice respectively from the Denver cell, further testing using a pneumatic cell was done. The goal is optimising the result with special focus on selectivity in small particle sizes. Reagent in g/ton for each step were kept constant. The grade-recovery results of PG FLOT are shown in Table 6 and Table 7. Initial flotation with a maximum of 71.12% (PG FLOT n) recovery was done. Recovery was later increased to 80.82% (PG FLOT r) with the addition of more ekofol. An initial poor recovery was compensated for by an incremental dosage of ekofol 452.

A comparison between these flotations and the Denver cell is shown in Figure 17

Table 6. Grade recovery without further recovery of residue.

Pneum. cell	Mass [g]	Mass [%]	mLoss(FC) 1000°C 1h [%]	Recovery [%]	Cumm. Grade [%]	Cumm. Rec. [%]
PG.FLOT n P1	38.92	1.46	97.11	1.57	97.11	1.57
PG.FLOT n P2	752.63	28.14	97.84	30.65	97.81	32.22
PG.FLOT n P3	958.56	35.85	97.50	38.90	97.64	71.12
Residue	924.02	34.55	75.08	28.88	89.84	100.00
∑	2674.13	100.00	89.84	100.00		

Table 7. Grade recovery with further recovery of residue.

Pneum. cell	Mass [g]	Mass [%]	mLoss(FC) 1000°C 1h [%]	Revovery [%]	Cumm. Grade [%]	Cumm. Rec. [%]
PG.FLOT r P1	38.92	1.46	97.11	1.57	97.11	1.57
PG.FLOT r P2	752.63	28.14	97.84	30.65	97.81	32.22
PG.FLOT r P3	958.56	35.85	97.50	38.90	97.64	71.12
PGFLOT r R1	240.11	8.98	96.99	9.69	97.56	80.82
Residue R2	683.91	25.58	67.39	19.18	89.84	100.00
∑	2674.13	100.00	89.84	100.00		

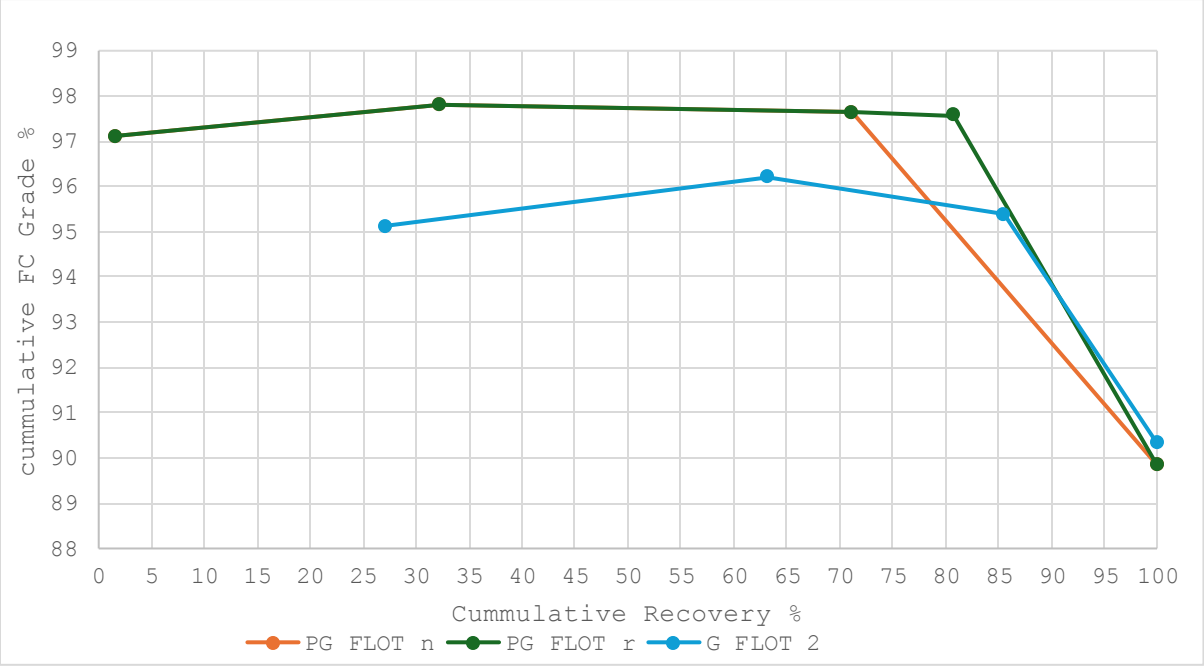

Figure 17. Comparison between GFLOT 2 and PG FLOT

4.3.3.3. PSD comparisons of graphite products and residues

The residues from the Denver and pneumatic cells (GFLOT 2 RES. and PGFLOT BOT., respectively) of the graphite flotation were finer than their respective products, with PGFLOT BOT. being finer than GFLOT 2 residues Figure 18 and Figure 19. This relatively shows an indication of entrainment of finer particles despite improved recovery from the pneumatic cell.

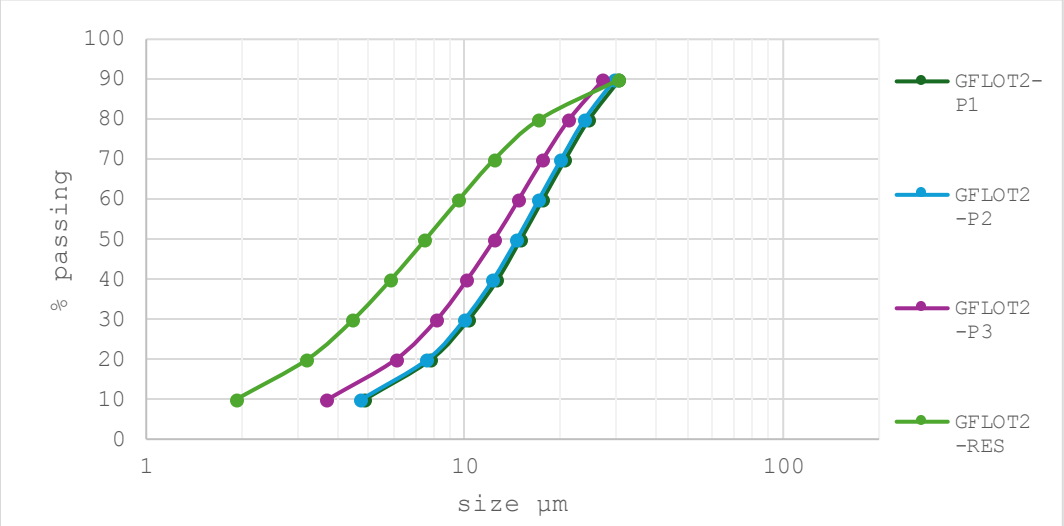

Figure 18. PSD GFLOT 2 of Denver cell flotation products and residues

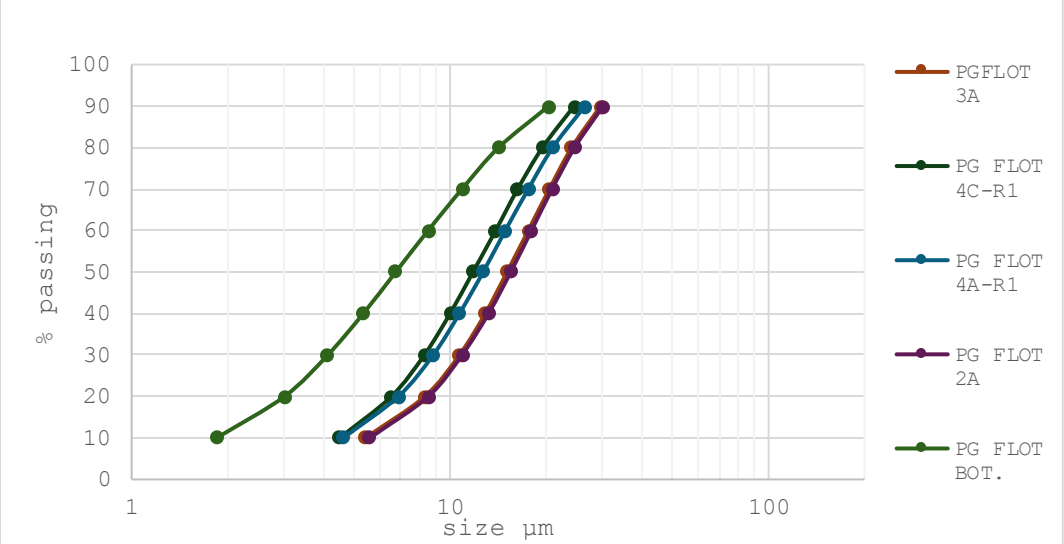

Figure 19. PSD of different pneumatic flotation products and residues

4.4. PyCP Purification

4.4.1. Goal

To find out the feasibility of flotation and settling velocity for the purification of PyCP, and also the extent of recovery of any paramagnetic material in the bulk.

4.4.2. Execution

An initial flotation test followed by settling velocity test was carried out for PyCP I reverse flotation and magnetic separation was used for PyCP II.

4.4.2.1. Mini-Denver flotation – PyCP I

A mini Denver cell with cell volume of 137.7 cm^3 and ekofol 452 reagent was used for an initial test for 2.5 volume percent of PyCP I. Hydrophobicity was reduced by the addition of alcohol (3.2, 4, 20, and 50% - Mflot 2-5).

For all descriptions, a single drop (0.009g) of ekofol 452 was initially used for conditioning for two minutes, which was followed by three drops after agitation for four minutes.

The product, due to its selectivity for the 50v% of ethanol, was dried, weighed, and an LOI test was conducted to check for carbon content.

4.4.2.2. Settling Velocity – PyCP I

The settling rate for the mixture of fine particles was done using 50 g of sample for sizes class 0.2/0.1 and <0.1 mm. Each weighed sample was dissolved in a 45g solvent of ethanol to improve dispersion and reduce hydrophobicity, thereby improving the singularity of grains in the fluid. The settling rate is the difference between single particle movement and that of the bulk.

The polyolefin sample consists of different elements and mineral phases. These different components have different densities and base on the Stokes equation (equation2), it shows that the settling rate is also based on the particle size and density.

$$V = \frac{d^2 g(\rho s - \rho f)}{18\mu} \qquad \text{equation (2)}$$

Where V is the settling velocity (m/s), d is the diameter of the particle (m), g is the acceleration due to gravity (m/s^2), μ is viscosity (Pas), ρ is the density (kg/m3) of solids and water.

Samples with defined upper and lower particle sizes were placed in a water column with a flow rate at a defined speed to allow low density particles to rise and high density particles to settle down.

The dispersed weighed sample of 50g in ethanol was discharged into the settling column at the given flowrate of 200L/hr and 80l/hr for size class 0.2/0.1mm and <0.1mm respectively. A total settling time of 15 min was used for both tests. The bottom and top contents of the column

were collected and filtered using a vacuum filtration set or a filter press depending on the volume.

The carbon content was also verified using the LOI test for carbon loss.

4.4.2.3. Flotation – PyCP II

An initial miniflotation check was conducted to determine if there is selectivity without the need for the addition of alcohol to improve solubility using 18g of sample. Two drops of ekofol were only used (one drop for each froth product), and a reasonable amount was floated after thorough mixing in the cell. Increased amount of materials were later used in the Denver cell by weighing 110g of the sample for the preparation of 5 v% concentration. Conditioning without any reagents was for 5 minutes. The froth product without any reagent was collected 5 minutes later. Two drops of ekofol were added, and the second froth product was collected in the 25th minute. This was followed by an additional three drops and a third product collected in the 35th minute. All products and residue were oven dried at 105^{o}C for 24 hours and LOI done.

4.4.2.4. Reverse Flotation – PyCP II

To reduce the ash content due to pyrolysis, a single stage reverse flotation of the sample was also done. Aero 3477 amine collector was used to promote the flotation of any silicates and ash using an amount equivalent to 1% weight of the PyCP; equivalent to 72 drops. Corn starch powder was used as a depressant for the carbon using the same 1% weight of PyCP equivalent to 1.1g while four drops of MIBC were used as a froth stabiliser. These reagents are based on similar ones used for the reverse flotation of lignite coal [72][73].

4.4.2.5. Wet Magnetic Separation – PyCP II

220g of dispersed sample in water was discharged into the flushed and cleaned system. This was after filling the matrix cylinder with water and ensuring there were no air bubbles in order not to obstruct the output signal [70]. A maximum current of 60A was used to obtain the strongest magnetic field.

The discharged materials were collected as non-magnetic products, while those left in the chamber (steel ball matrix in the cylinder) within the electric field are collected as magnetic materials. Products were analysed using a Satmagan and LOI. The wet magnetic process is also more effective than the dry process for materials with weaker magnetic properties and finer particle sizes [71]. The magnetic property is compared based on that of magnetite by using a Satmagan Figure 7(b) This comparison is based on the paramagnetic properties due to the

existence of unpaired electrons, which are responsible for the material's magnetic behaviour. Unpaired electrons in pyrolytic carbon come from imperfections and impurities in the material, such as dangling bonds and vacancies [77].

4.4.3. Results and Discussion – PyCP Purification

4.4.3.1. PSD of bulk PyCP

The PSD distribution for PyCP I is as shown in Figure 20, with fifty percent of the materials <2mm. This distribution is as received before the milling process. The milling process was necessary due to agglomerations.

For PyCP II Figure 21, 93% of the bulk sample is less than 100µm. This difference in distribution confirms the effect of pyrolysis oil, as seen with PyCP I.

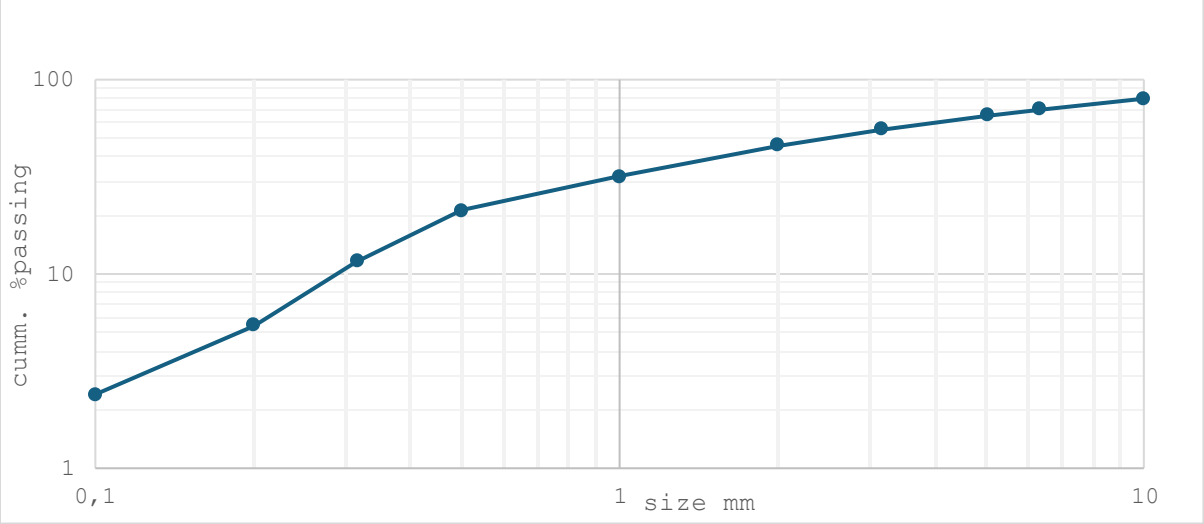

Figure 20. PSD of bulk PyCP I

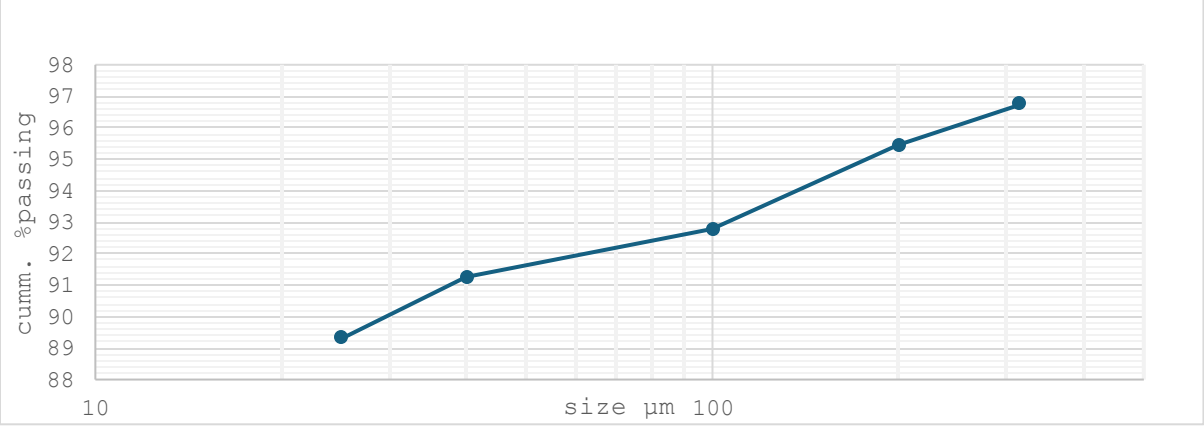

Figure 21. PSD of bulk PyCP II

4.4.3.2. PSD of PyCP <100µm

For all samples, the size class is considered to be <100µm; however, the PyCP sample I (18.4–174µm) shows a great difference in distribution when compared to sample II (1.1–12µm) Figure 22. The higher size classes, as observed from sample I can be due to non-thorough sieving or agglomeration due to the presence of residual oil and different definition of particle size based on techniques used.

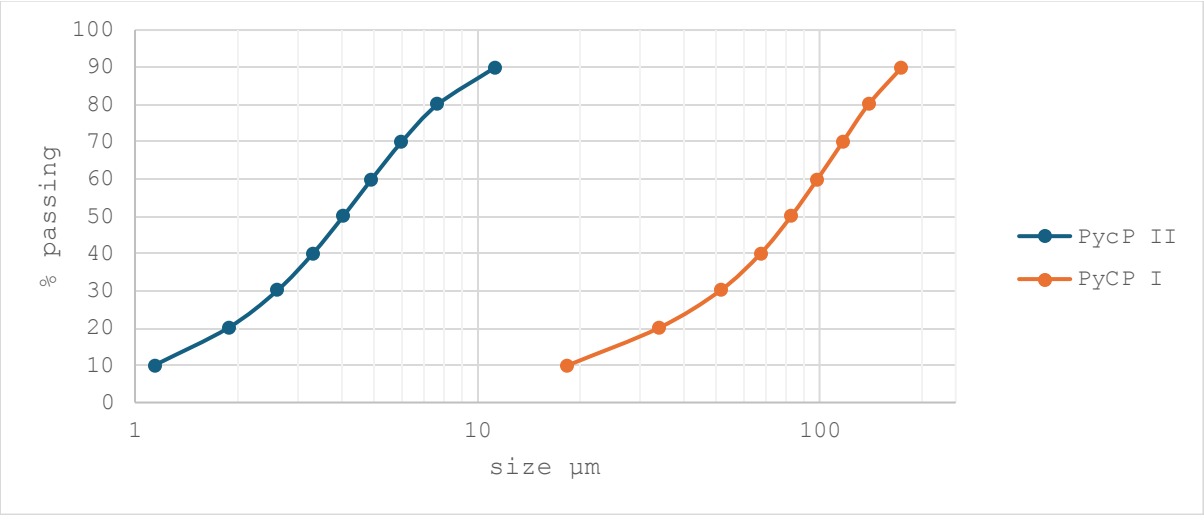

Figure 22. PSD of PyCP <100µm

4.4.3.3. LOI of bulk of PyCP I and II

The carbon content of the bulk feed for PyCP I based on the different size classifications is as given in Table 8.

Table 8. Carbon Content of Bulk PyCP I

size (mm)	%carbon
>10	48.23
10/6.3	57.66
6.3/5.0	50.51
5/3.15	52.24
3.15/2.0	51.80
2/1.0	51.14
1/0.5	50.33
0.5/0.315	50.47
0.315/0.2	49.23
0.2/0.1	48.61
<0.1	48.40

The carbon contents for the different size classes of PYCP II are as shown in Table 9

Table 9. Carbon content of PyCP II

size (µm)	%carbon (LOI)
>315	59.71
315/200	62.42
200/100	62.46
<100	60.11

From Table 9 above, we have on average, a higher carbon content for each size class when compared to that of PyCP I.

4.4.3.4. Image Analysis

Microscopic image analysis from Figure 23 and Figure 24 for pyrolytic polyolefins of bulk <500µm showed that there is a mix of other materials in the sample.

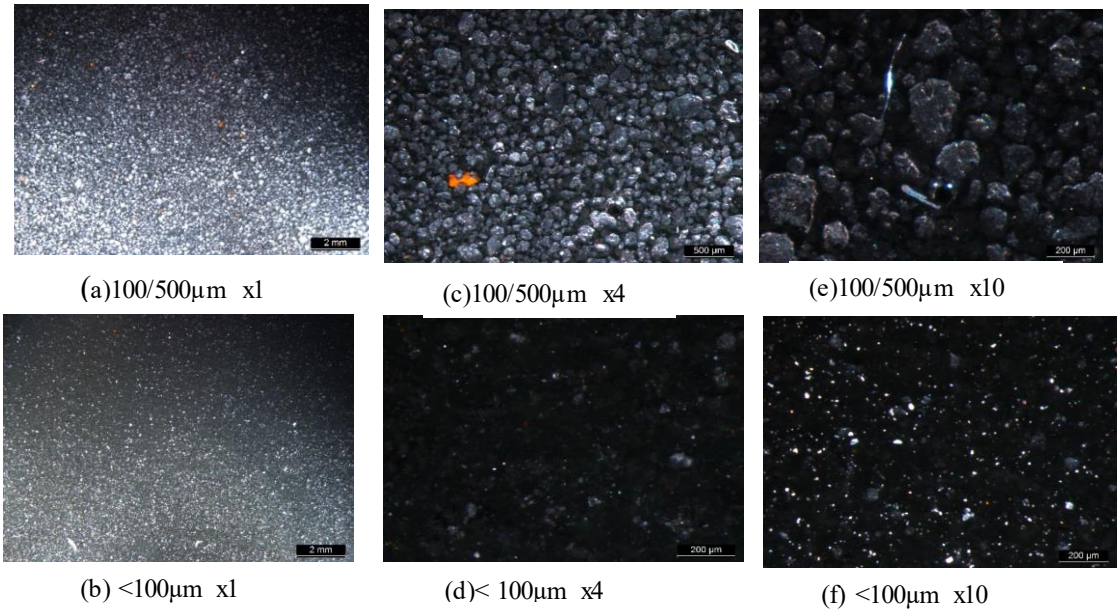

(a)100/500µm x1 (c)100/500µm x4 (e)100/500µm x10

(b) <100µm x1 (d)< 100µm x4 (f) <100µm x10

Figure 23. Stereo images of pyrolytic polyolefins with different magnifications

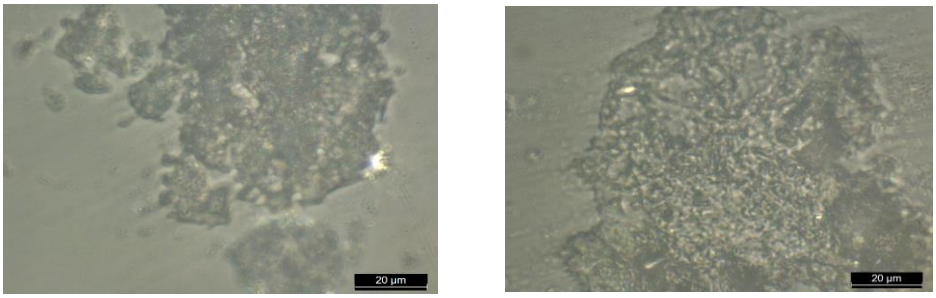

(a) <100µm x4 (b) 100/500µm x4

Figure 24. Point focused image analysis of Leica MC170 HD

4.4.3.5. Mini Flotation of PyCP I

The flotation for selectivity of carbon in a mini-Denver cell was done; low alcohol tests didn't achieve any results as the whole sample was reported to the froth product. The results of the only test with separate froth product and residue for the 50% alcohol dissolution are shown in Table 10.

Table 10. Cumulative grade (carbon content) after flotation of <100µm – MLOT 5

Mini Cell	Mass [g]	Mass [%]	m_{Loss} 1000°C 1h [%]	Recovery [%]	Cumm. Grade [%]	Cumm. Rec. [%]
M.FLOT 5 FP1	0.9	17.6	49.1	17.8	49.14	17.8
M.FLOT 5 FP2	1.6	30.8	49.3	31.2	49.22	49.0
Residue FP3	2.8	51.6	48.1	51.0	48.65	100.0
∑	5.3	100.0	48.6	100.0		

Despite the addition of 50% alcohol, there was still a problem of selectivity as there was hardly any flotation, and the carbon grade remained almost the same 49.22 and 48.65% for the product and feed, respectively.

4.4.3.6. Mini Flotation of PyCP II

Also, based on Table 11, there isn't any improvement in the grade of the products either (59.39%), but improvement was seen in the residue (63.45%), a possible indication that other non-combustible materials readily float in comparison to the carbon. A further test was done in the Denver cell to verify this.

Table 11. Flotation products of mini-Denver cell for PyCP II

Mini Cell	Mass [g]	Mass [%]	m_{Loss} 1000°C 1h [%]	Recovery [%]	Cumm. Grade [%]	Cumm. Rec. [%]
M.FLOT SII P1	4.75	54.10	58.97	52.96	58.97	52.96
M.FLOT SII P2	2.20	25.06	60.29	25.08	59.39	78.04
Residue	1.83	20.84	63.45	21.96	60.23	100.00
∑	8.78	100.00	60.23	100.0		

4.4.3.7. Denver Flotation of PyCP II

The Denver flotation results are shown in Table 12, verifies that of the mini cell, the carbon content of the residue (62.8%) is also higher than that of the cumulative products (58.87%).

Table 12. Flotation products of Denver cell for PyCP II

Denver cell	Mass [g]	Mass [%]	$m_{Loss(FC)}$ 1000°C 1h [%]	Recovery [%]	Cumm. Grade [%]	Cumm. Rec. [%]
P.FLOT FP1	4.63	4.35	59.39	4.30	59.39	4.30
P.FLOT FP2	26.23	24.66	58.89	24.16	58.97	28.47
P.FLOT FP3	42.18	39.65	58.79	38.79	58.87	67.26
Residue	33.33	31.33	62.80	32.74	60.10	100.00
∑	106.37	100.00	60.10			

4.4.3.8. Reverse Flotation of PyCP II

The reverse flotation (Table 13) shows that the carbon grade can be improved by depressing the carbon while floating ash. A higher grade of 66.66% even with a higher recovery of 81.47% of the froth products. This situation is similar to that of coal, as explained by Özturk [74], in that the ash content is based on the gray value and can be reversely floated. This relationship between the ash content and the gray value due to its dark coloration (an indication of carbon content) is a direct one [75]. Also, the use of a suitable frother prevents bubble coalescence and improves froth stability [76] based on observation when MIBC is used in the fourth product of the reverse flotation.

Table 13. Reverse flotation products of Denver cell for PyCP II

Denver cell	Mass [g]	Mass [%]	$m_{Loss(FC)}$ 1000°C 1h [%]	Recovery [%]	Cumm. Grade [%]	Cumm. Rec. [%]
R.FLOT P1	13.14	12.52	58.47	12.18	58.47	12.18
R.FLOT P2	16.71	15.92	58.57	15.51	58.53	27.69
R.FLOT P3	13.47	12.83	58.40	12.47	58.49	40.16
R.FLOT P4	44.11	42.02	59.10	41.31	58.80	81.47
Residue	17.54	16.71	66.66	18.53	60.11	100.00
∑	104.97	100.00	60.11			

The table of analysis for the LOI values of all samples for magnetic separation, mini-Denver, and Denver cell flotation for PyCP II are shown in Appendix 3

4.4.3.9. Magnetic Separation of PyCP II

Based on this analysis in Table 14 the sample can be considered to be paramagnetic due to the low mass percent of the magnetic component, with a total recovery of just 18.53%. Also, a doubling of the satmagan value of the feed would have suggested enrichment of non-combustibles in the magnetic product, but there wasn't any change in grade for both feed and magnetic or non-magnetic components based on LOI.

Table 14 Magnetic separation balance

	mass(g)	Mass %	% magnetite	mLoss(FC)%	Recovery%
Mag	19.22	9.12	0.68	59.57	18.53
N Mag	191.49	90.88	0.30	59.65	81.47
Feed	210.71	100.00	0.33	59.64	100.00

4.4.3.10. Settling Velocity of PyCP I

Table 15 shows the percent carbon from settling velocity. Flocculation rather than selectivity was achieved. A look into the elemental composition from a handheld XRF Table 2 also indicates that there is a considerable amount of Si, Ca, Ti, Fe, and Mg present in the sample which still seems to be evenly distributed between the products.

Table 15. Settling velocity % carbon and mass

Size(mm)		Mass (g)	recovered mass	% carbon
0.2/0.1	Top	11.58		53.08
	Bottom	26.79	38.37	52.92
<0.1	Top	4.61		52.31
	Bottom	36.54	41.15	52.98

4.5. Agglomeration of CMP

4.5.1. Goal

Determining the best mix of binder and moisture content for tumble and pressure agglomeration of CMP.

4.5.2. Execution

The agglomeration process of the CMP was by tumble growth using a mixer granulator and pressure agglomeration using a cold press mechanism.

4.5.2.1. Mixing and Granulation

The total mass of carbon plus binder is maintained at 300 g, while water content of 40% was set for all samples. The following steps were done for each experiment:

- Mixing for 1 minute at medium speed with the addition of water

- Granulation for 4 minutes at high speed
- Granulate further for 2 minutes at low speed

All the granules were then dried in the oven at 105°C for 24 hours.

Detailed sample descriptions are given in Table 16, all clay binders except for sample I (dry mix) are mixed with water before application to the CMP.

Table 16. Sample descriptions of the different binders mix

sample	**mixture by weight percent**	**Carbon + binder**	300g
A	CB (100%) + water (40%)	water = wt% of **carbon + binder**	
B	CB (97%) + lignosulfonate (3%) + water (40%)		
C	CB (99%) + lignosulfonate (1%) + water (40%)		
D	CB (97.67%) + corn starch (2%) + NaOH (0.33%) + water (40%)		
E	CB (98.99%) + corn starch (1%) + NaOH (0.00165%) + water (40%)		
F	CB (90%) + Clay (10%) + water (40%)		
G	CB (80%) + Clay (20%) + water (40%)		
H	CB (70%) + Clay (30%) + water (40%)		
I	CB (70%) + Clay (30%) + water (40%)		

4.5.2.2. Sieving

The following size class of 10, 6.3, 5 4,3.15,2 and 1mm and their respective sieves were used for particle size distribution. Figure 25 shows some granules obtained.

Figure 25. Granules from tumble growth agglomeration

4.5.2.3. Compressive Strength test

Granules of sizes between 5 and 3.15 mm in diameter were selected for this test. Breakage force and compressive strength test was done for five trials using the Messphysik MIDI 10 press.

4.5.2.4. Pressure Agglomeration

Mixing of the CMP and 3 wt% lignosulfonate binder was done based on first dry mixing at medium speed and 1 minute at high speed for wet mixing in the Eirich mixer-granulator. This was done for weight percents of 5, 10, 15, 20, 25, 30, 35, and 40 of water, and a total of 108g was removed for three trials of pressure agglomeration for each.

Pressure agglomeration by compaction at a maximum force of 3500 N was carried out on each mix. The bed depth of 7.5cm and diameter 2cm of the die was maintained throughout each test while the compacting speed was at 10 mm/min. The density of each pellet was calculated by:

$$\rho = \frac{m}{\pi r^2 l} \qquad \text{equation.(3)}$$

Where ρ is the density (g/cm3), m is the mass of the pellet (g), r is the radius (cm) and l is the length (cm).

The weight and height of each press were measured and placed in a dryer at 105°C for 24 hours. A diametral compression test was done using a piston for compression on a rigid cylinder with a flat surface of diameter 15cm and at a speed of 1mm/min. The applied force and displacement are gotten from the readings of a computer connected to the press. Following the procedure of diametral compression, the compressive strength which is applied perpendicular to the cylindrical axis as described is given by equation (4) below.

$$C.S = \frac{10BF}{\pi r l} \qquad \text{equation.(4)}$$

Where C.S is the compressive strength (KPa), BF is the breakage force (N), r and l are the radius (cm) and length (cm) of the cylindrical pellet respectively.

Samples of pellets produced as seen in Figure 26 was maintained for the die depth for all variations of binders used and water content.

Figure 26. Sample of pellet produced from pressure agglomeration.

A second set of pressure agglomerations were further experimented on using Diatomaceous Earth (DE), a commonly used filtration aid in breweries, as a binder. The DE used was completely dispersed in water and stirred to ensure complete suspension. The pulp density was calculated by weighing 1000ml of the suspension. This gives a density of 1.048g/cm3. The mass percent of the DE from the pulp (7.88%) was used to calculate the mass of pulp expected to contain the needed dry mass of DE; this is considered the weighed pulp. The required mix (dry mass plus 23 wt% moisture) was selected for the weight percent of DE (8.7, 15, 20, and 8.7% DE with 10% clay). The excess water between the weighed pulp and calculated pulp was then decanted out.

The final pulp was added to the dry mass and mixed in the Eirich Mixer granulator using the same set point as that of lignosulfonate.

A table of descriptions is given in Table 17. It is observed that for 15 and 20 wt% of DE, the moisture content attained was 25%. This is because the higher the DE, the more water is absorbed, thereby reducing the amount of water to be decanted.

Table 17. Calculated weight of DE pulp required.

			Total dry mass (mtot)		300	clay dry(10% of mtot)		30
			wt % water		23%	wt% of DE pulp		7.88%
wt% of DE	mass DE (g)	mass of water(g)	required mix (g)	weighed pulp(g) (calculated)	water to be removed (g)	actual water removed (g)	excess water (g)	actual wt% water
8.7%	26.1	89.61	115.71	331.22	215.51	215.51	0.00	**23%**
15%	45	89.61	134.61	571.07	436.46	393.38	43.07	**25%**
20%	60	89.61	149.61	761.42	611.81	545.49	66.32	**25%**
8.7% +10%CLAY	56.1	89.61	145.71	331.22	185.51	185.51	0.00	**23%**

4.5.3. Results and Discussion for CMP Agglomeration

4.5.3.1. PSD of CMP relative to bulk feed

The relative fines of all bulk feed are less than 100µm. PyCP II and CMP showed similar distributions and extents of fines, with over 90% less than 11 µm. PyCP II and CMP still have finer size class materials when compared to the residues of the pneumatic flotation cell. These are shown in Figure 27.

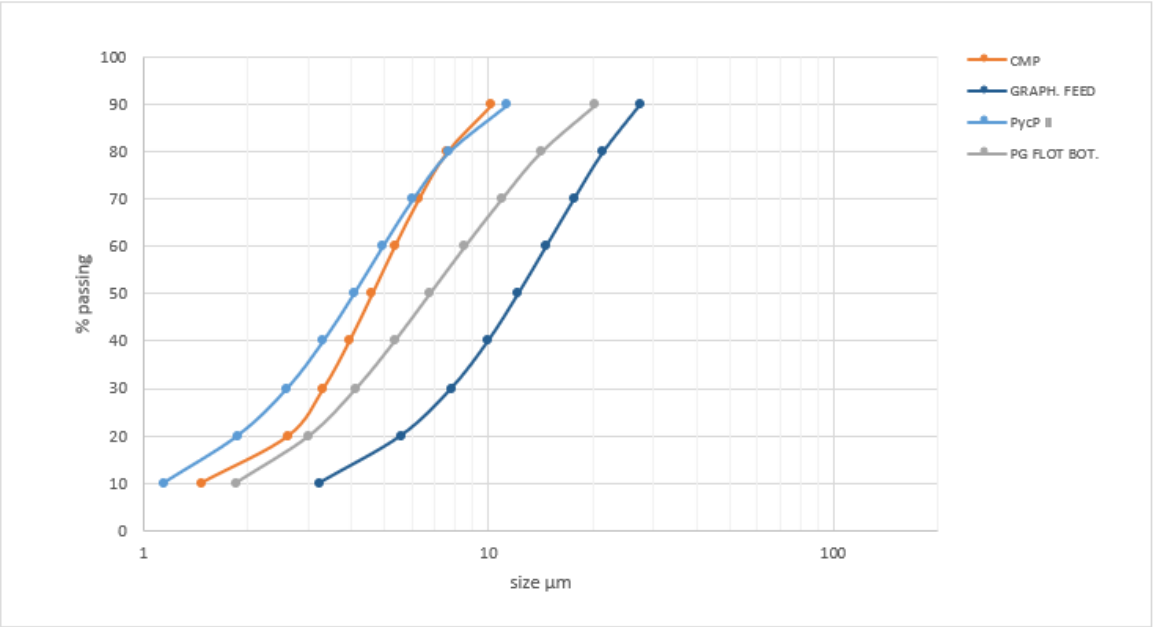

Figure 27. PSD of CMP, PyCP II and graphite feed and residue.

4.5.3.2. PSD of granules

Sieve analysis of granules of samples are shown in Table 18. There is no distribution for samples H and I because lumps instead of granules were formed, an indication of excessive clay content above 20 wt%. The PSD of the various granules is given in Figure 28.

Table 18. Amount attained for each sample (g)

size(mm)	A	B	C	D	E	F	G
10	1.87	75.26					
6.3	4.88	100.89					
5	2.00	22.04				8.30	41.58
4	2.47	6.12	3.21	3.47		33.71	76.67
3.15	2.97	14.79	8.02	21.90	20.17	41.42	34.73
2	25.02	38.46	96.91	96.00	53.61	85.55	38.18
1	85.02	27.46	101.20	56.27	65.11	55.01	23.53
0	70.63	11.59	10.49	11.11	41.50	46.70	42.37
Total	**194.86**	**296.61**	**219.83**	**188.75**	**180.39**	**270.69**	**257.06**
% loss(stickiness)	35.05	1.13	26.72	37.08	39.87	9.77	14.31
% loss(attrition)	23.54	3.86	3.50	3.70	13.83	15.57	14.12

Stickiness was highest for sample E during granulation and resulted in a 39.87% loss during granulation. This can be attributed to the poor mechanical behaviour and high water vapour permeability, which are the main drawbacks of starch-based materials [63]. Furthermore, when compared with sample D, the NaOH content is negligible; therefore, it can be assumed that only corn starch was used. Attrition loss occurred most with sample A due to the absence of any binder.

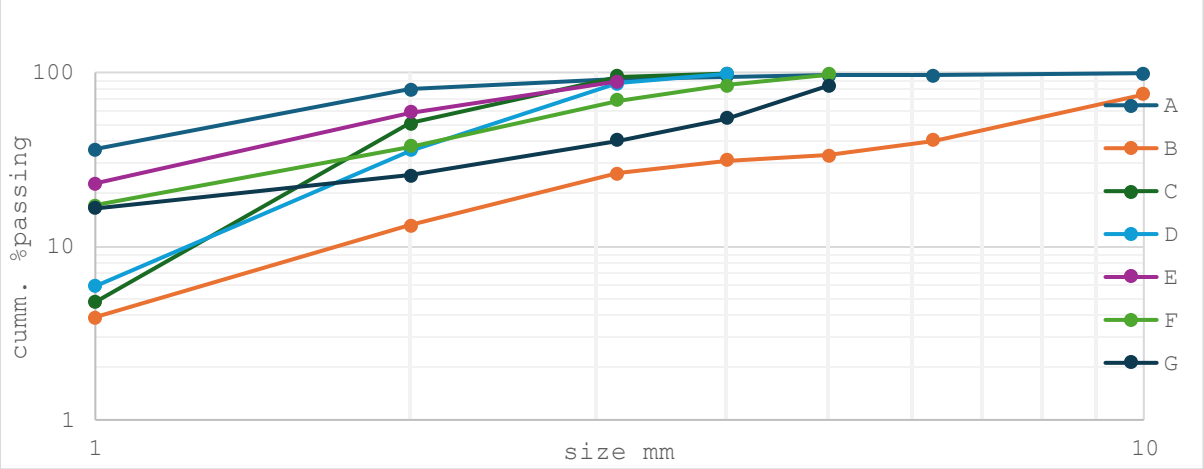

Figure 28. PSD of granulated CMP

From Figure 28, only samples A and B have size classes across all ranges of sieves used as an indication of properly distributed agglomerates, with sample A having finer materials than sample B with P50 < 2mm and P50 < 7 mm, respectively.

4.5.3.3. Compressive Strength Test of Granules

The BF of each size classes in consideration are shown in Figure 29

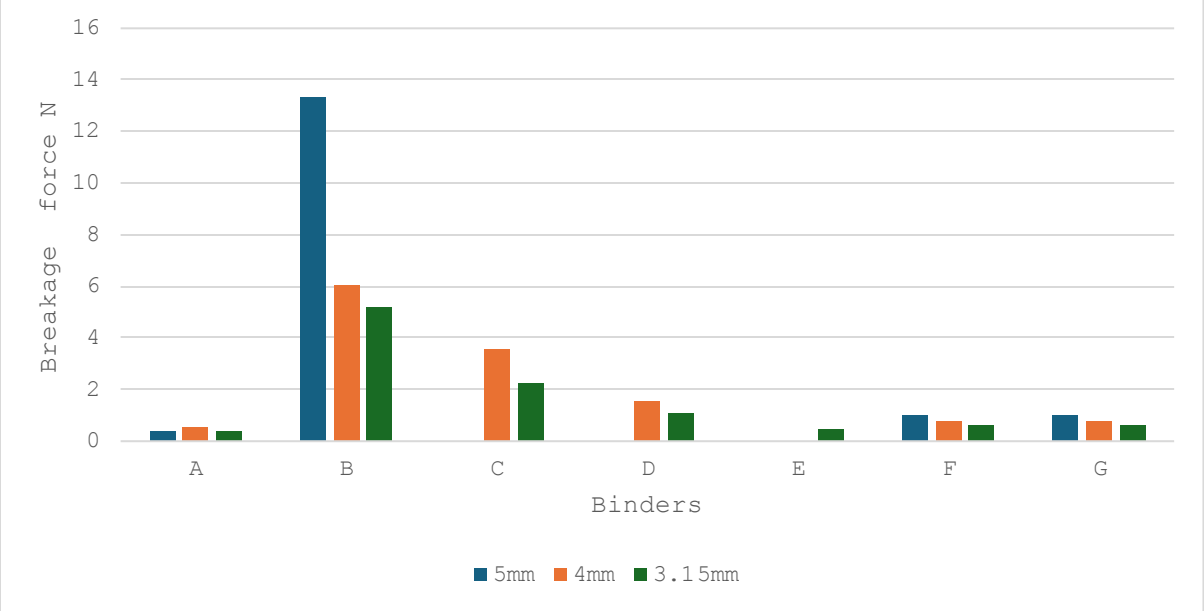

Figure 29. Breakage force of granule samples

The BF required for sample B for all size classes measured is higher than that of others. This is also true for the compressive strength on each granule for the different samples and sizes in Figure 30.

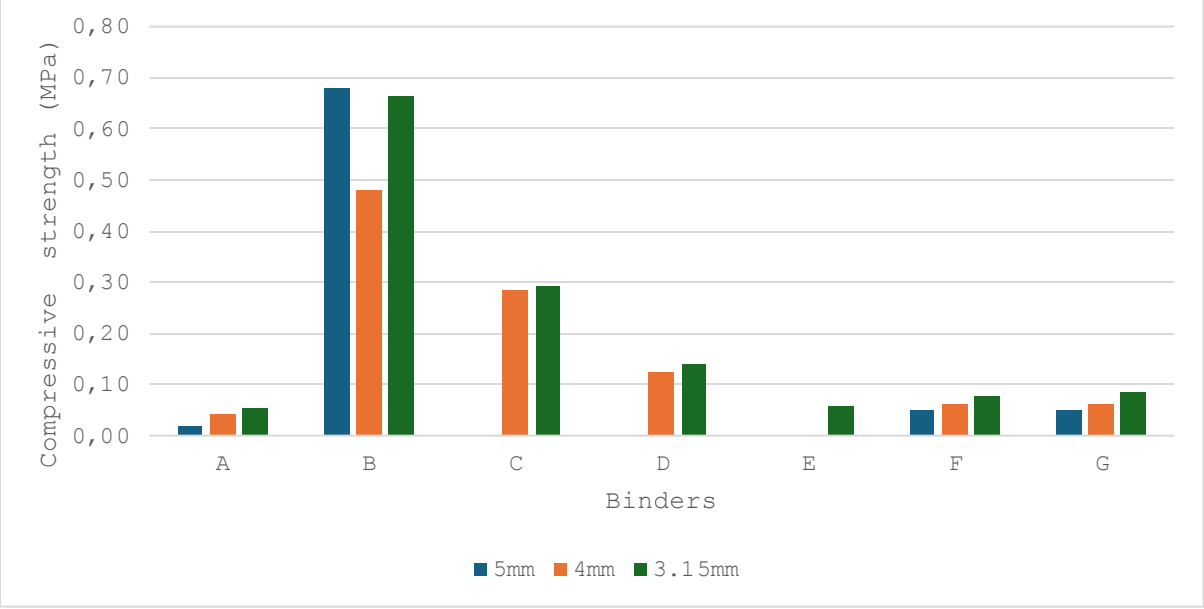

Figure 30. Compressive strength by size class for each granule sample

Table 19. % change in BF and CS with A as reference for granules

size(mm)	A	B	C	D	E	F	G
5	0	3343.81				151.80	161.34
4	0	994.92	552.81	187.66		42.65	38.48
3.15	0	1100.56	429.55	149.42	6.30	37.33	51.92

Generally, as shown in Table 19, the change in BF and CS reduces with the size except for 3.15mm of sample B due to the close proximity of the required BF with the 4mm and reduced area.

4.5.3.4. Pressure Agglomerates from using sample B and varying wt% water.

Pressure agglomeration by cold pressing was only carried out for sample B since it gives the best strength for the granules. Also, it gave the best CS results for granules in the tumble growth agglomeration process.

The results are shown in Table 20 and Figure 31. The full details of the individual test are shown in Appendix 4**.**

Table 20. CS test of pellet for different moisture content for 3 wt% lignosulfonate binder

wt% of water	BF (N)	CS (Kpa)	mass of water(g)	% mass of water	Length of press – L (cm)	density(g/cm3)	L/D
5%	8.83	18.33	0.04	0.98	1.53	0.842	0.77
10%	19.69	40.00	0.02	0.53	1.57	0.931	0.78
15%	47.75	64.22	1.17	18.66	2.37	0.843	1.18
20%	65.52	80.21	1.90	26.43	2.60	0.878	1.30
25%	64.95	82.70	2.13	32.62	2.50	0.833	1.25
30%	56.15	60.93	3.23	40.98	2.93	0.856	1.47
35%	65.00	55.92	4.80	50.19	3.70	0.823	1.85
40%	27.86	25.34	4.28	48.13	3.50	0.806	1.75

The BF and CS increased with moisture content until moisture content reached 25% before they started reducing. A sharp increase in the BF for moisture content of 35% was observed, however, this is considered a measurement error due to the high variance between the individually measured values from Appendix 5.

It is also observed that the length of the cylindrically pressed agglomerate increases as the moisture content increases upon extrusion. It is expected that the BF increases as the L/D (length /diameter) ratio increases [57]. However, this cannot be the case because, with

increasing moisture content, the strength of the pellet also reduces. However, there is a generally slight decrease in densities as the L/D ratio increases, although this is not uniform due to slight differences in compaction. Figure 32 shows the density and length of pellet relationships with density remaining almost constant regardless of variation in length of pellet.

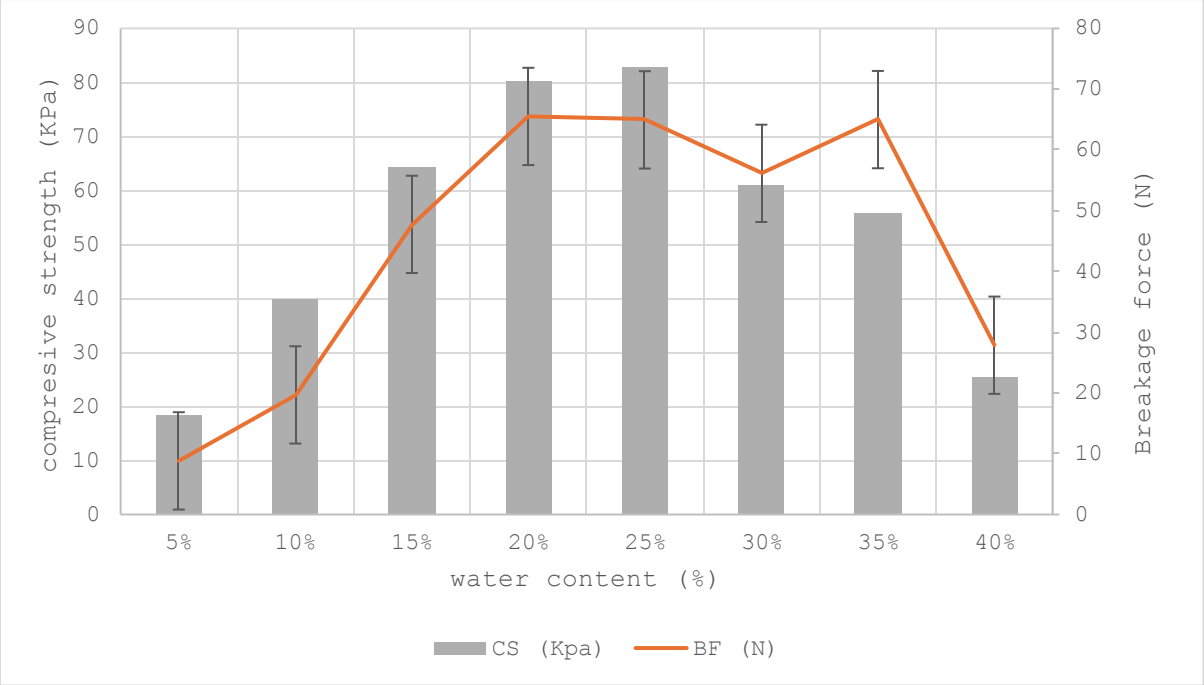

Figure 31. Average CS and BF for varying moisture of sample B

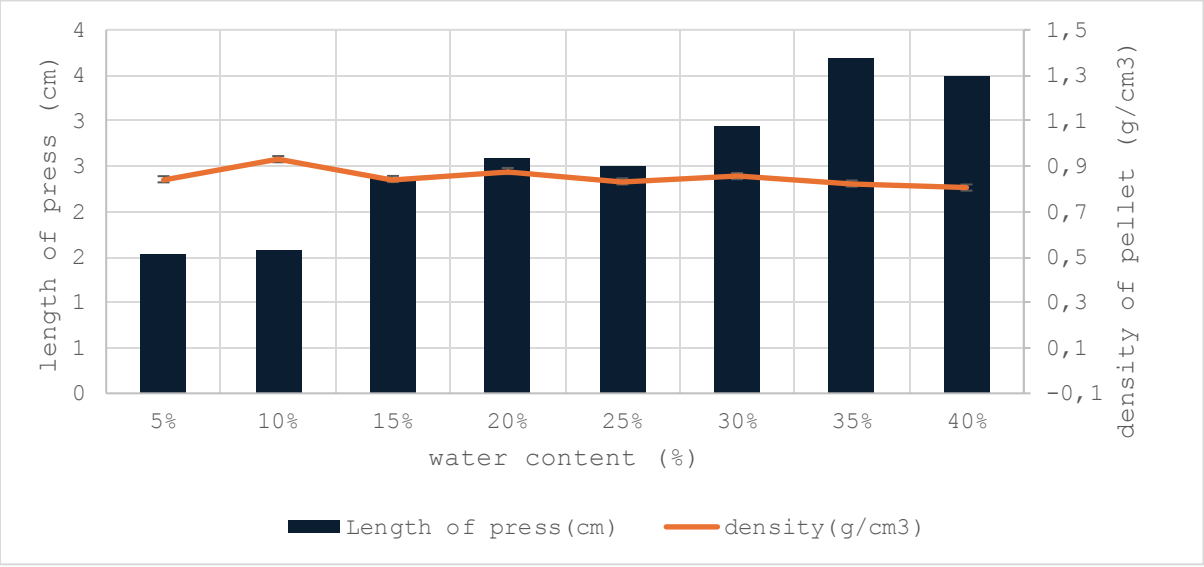

Figure 32. Density and length of pellet relationships

4.5.3.5. Pressure Agglomerates from using Sample B and 23 wt% water of DE

The repeated process using DE as a binder gives the following results in Table 21.

Table 21. Pressure agglomeration for BF and CS using a cylindrical die for varying wt% DE.

wt% of DE	BF (N)	CS (Kpa)	mass of water(g)	% mass of water	length of press (cm)
8.7%			1.51	27.80	2.00
15%	21.01	23.89	2.63	36.89	2.80
20%	29.77	31.59	3.43	43.31	3.00
8.7% (DE) +10% CLAY	0.50	0.61	1.53	24.34	2.60

The table of individual measurements is shown in Appendix 6. There isn't any value for BF or CS because, at 8.7% DE, the strength is very small and cannot be read. A similar observation was noticed with the 8.7% DE + 10% CLAY mix, BF is very small, resulting in low stress. Also, the length of the press increases as the moisture content increases due to the increased amount of DE. This can also be explained for the 8.7% DE + 10% CLAY mix, as the addition of clay results in a slightly higher amount of water.

It was also observed that the smoothness of the press was less than that of sample B. This roughness is attributed to the presence of silica in the DE and clay, which is also the cause of the reduced strength of the press. Figure 33 shows the average CF and stress for various wt% of DE.

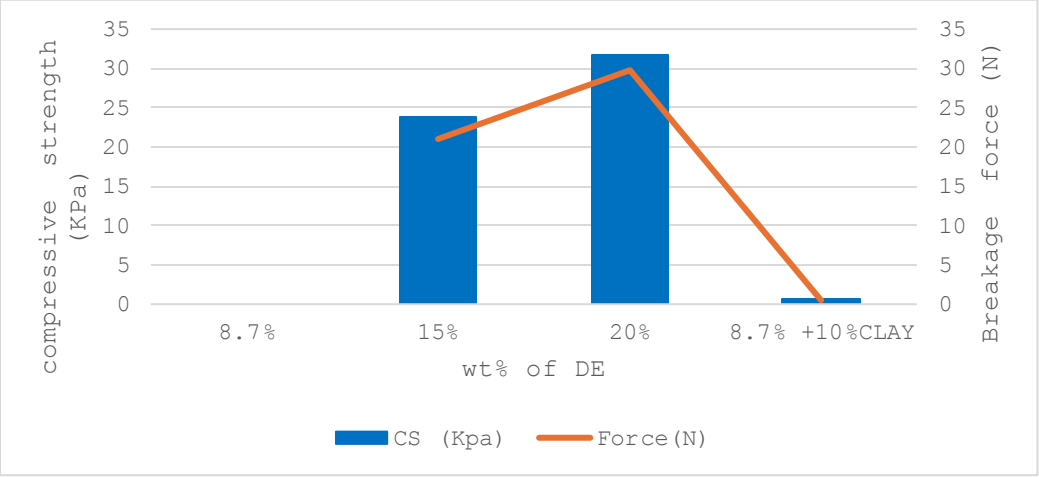

Figure 33. BF and CS for various wt% of DE

Chapter 5: Conclusion and Recommendations

5.1. Conclusion

The characterization results based on PSD for the PyCP show that the influence of pyrolytic oil greatly reduces the fineness due to re-agglomeration. Furthermore, pyrolytic carbon from methane- CMP, is considered the finest of all forms of pyrolytic carbons observed and also finer than residues from flotation of processed graphite. This can be attributed to the fact that CMP is a pure carbon product from a decomposition reaction of methane without any other foreign materials or oil, as observed for the processed graphite and PyCP. The higher surface area of the PyCP can be attributed to the porosity of the PyCP being higher than that of the CMP. Microscopic image analysis indicated that there are impurities in the PyCP, hence the need for purification.

The purification methods used were focused mainly on the PyCPs since they contain impurities and are produced under varied pyrolytic conditions. The preflotation test for PyCP I and II showed that there wasn't any selectivity for PyCP I probably due to the pyrolytic oil acting as a collector. On the other hand, the selectivity observed for PyCP II was in the reverse manner than expected. Therefore, a reverse flotation mechanism was observed to give some improvement in the grade. Furthermore, the modelling of this flotation using graphite isn't feasible since it works best in reverse flotation.

Other physical purification processes, such as magnetic separation for PyCP II and settling velocity for PyCP I, indicated no significant change in the carbon grade but there was the presence of paramagnetic materials from the wet magnetic separation process.

Agglomeration was done using CMP. For the agglomeration process, a 3 wt% lignosulfonate with 40% water - sample B performs best amongst all types of binders used with respect to BF and CS. The preferred size class for the handling of granules of this type was in the range of 5–3.15 mm for better handling due to the effect of tensile stress in the lower size class, which results in attrition losses.

The desired size of interest for handling purposes will largely depend on its strength and the size suitable for its applications.

The pressured agglomerate of the 3wt% lignosulfonate binder is best pelletized with a moisture content of 23%. A further increase in the moisture content resulted in an increased length of the press upon extrusion, and an increased L/D ratio, which slightly reduced the density of the pellets.

The compressive strength of the pressed agglomerate using DE is always less than that of 3 wt% of lignosulfonates, even at the same moisture content of 23%. Also, the retention of more moisture due to the absorption of water when the amount of binder increases makes fixing a particular moisture content difficult for varied DE content. Pellet sizes are often longer and rougher when compared with those of lignosulfonate binder.

5.2. Recommendations

More advanced characterization analysis, such as scanning electron microscopy and thermogravimetric analysis of the feed and products after purification, will give a more detailed characterization of the PyCP.

Furthermore, the focus should be on the pyrolytic conditions during the pyrolysis process for better PyCP with no oil. Also, the modelling of the flotation of PyCP should be done with coal for reverse flotation rather than graphite.

Other forms of pressing and extrusion techniques can still be explored for a better pelletization process. Further research work on using DE and lignosulfonate as binders is highly recommended for agriculture since they improve soil enrichment and the strength of the pellet, respectively.

Chapter 6: Summary

The objective of this thesis is to investigate various carbons from pyrolysis by characterization, purification, and to improve handling through agglomeration. The pyrolytic carbons investigated are carbons from polyolefins (PyCP) and carbon from methane pyrolysis (CMP). In addition to these, flotation of a naturally occurring carbon, graphite, as a possible model for the flotation of PyCP was investigated. The graphite flotation was done in a Denver as well as an allminerals pneumatic cell for grade improvement and an enhanced recovery process.

The PyCP consisted of two bulk samples (I and II) with varying degrees of pyrolysis, with PyCP II more pyrolyzed than PyCP I and with insignificant amounts of pyrolytic oil when compared with PyCP I. Image analysis and PSD of bulk samples were done for characterization, while purification tests of flotation, settling velocity, and wet magnetic separation were done to check for the most feasible process for improving the carbon content of the sample. Reverse flotation of PyCP II was considered the best option for purification due to its improved carbon grade in comparison with other purification processes used. Purification by floatation or settling velocity for PyCP I was difficult due to the presence of pyrolytic oil, which leads to flocculation and lifts all components regardless of individual surface properties.

The agglomeration tests on CMP using tumble growth agglomeration and pressure agglomeration by the cold press mechanism. Various binders were tried for tumble growth agglomeration to determine the most suitable binder at a fixed moisture content of 40%. The best binder observed was lignosulfonate at 3 wt% which was used for pressure agglomeration at varying moisture content.

The major challenges encountered during this work are difficulty in dispersing PyCP I even when dissolved in alcohol, the oil leads to flocculation and during flotation, lifts all components regardless of individual surface properties. Therefore, it is always best if PyCP is completely pyrolyzed removing any residual oil before other purification steps can be carried out. For pressure agglomeration, the stability and compressive strength improved significantly above 10% water content with an optimum at 25%.

Separation by flotation was done for two samples of PyCP (I and II) with different degrees of pyrolysis, and the presence of residual pyrolysis oil for PyCP I and no oil for PyCP II. Flotation was not feasible for PyCP I as selectivity was poor while the flotation of PyCP II was best done by reverse flotation, with a carbon grade of 66.66% compared to 60.1% of the feed. The purification by settling velocity didn't give any significant improvement in the carbon grade, while an 18.53% recovery of magnetic materials was attained from the wet magnetic process.

A handling test after agglomeration for the CMP was by evaluating the compressive strength (CS) and breakage force (BF). A 3 wt% of lignosulfonate binder and 40 wt% water was used for the tumble growth agglomeration. The breakage force (BF) for the median size classes of 5, 4, and 3.15 mm of the granules is 13.36, 6.03, and 5.18 N. The optimal moisture content for pressure agglomeration was attained at 25 wt% water with a BF and CS of 64.95N and 82.7Kpa using the same weight percent of lignosulfonate. A similar experiment for diatomaceous earth (DE) as a binder was also done, but with less CS and BF when compared to lignosulfonate, even with varying amounts of DE.

References

[1] L. Lombardi, E. A. Carnevale, and A. Corti, "A review of technologies and performances of thermal treatment systems for energy recovery from waste," *Waste Management*, vol. 37, pp. 26–44, Mar. 2015, doi: 10.1016/j.wasman.2014.11.010.

[2] R. A. Witik *et al.*, *CARBON FIBRE COMPOSITE WASTE: A Comparative Assessment of Recycling and Energy Recovery*. 2012. [Online]. Available: http://www.escm.eu.org/eccm15/data/assets/1660.pdf

[3] P. Das and P. Tiwari, "Valorization of packaging plastic waste by slow pyrolysis," *Resources, Conservation and Recycling*, vol. 128, pp. 69–77, Jan. 2018, doi: 10.1016/j.resconrec.2017.09.025. 10.1016/j.wasman.2014.11.010

[4] M. Syamsiro *et al.*, "Fuel Oil Production from Municipal Plastic Wastes in Sequential Pyrolysis and Catalytic Reforming Reactors," *Energy Procedia*, vol. 47, pp. 180–188, Jan. 2014, doi: 10.1016/j.egypro.2014.01.212.

[5] B. Fekhar, V. Zsinka, and N. Miskolczi, "Value added hydrocarbons obtained by pyrolysis of contaminated waste plastics in horizontal tubular reactor: In situ upgrading of the products by chlorine capture," *Journal of Cleaner Production*, vol. 241, p. 118166, Dec. 2019, doi: 10.1016/j.jclepro.2019.118166.

[6] S. Psomopoulos, K. Kiskira, K. Kalkanis, H. C. Leligou, and N. J. Themelis, "The role of energy recovery from wastes in the decarbonization efforts of the EU power sector," *IET Renewable Power Generation*, vol. 16, no. 1, pp. 48–64, Oct. 2021, doi: 10.1049/rpg2.12315.

[7] S. Gibbens, "How global warming is disrupting life on Earth," *Environment*, Feb. 14, 2024. [Online]. Available: https://www.nationalgeographic.com/environment/article/global-warming-effects. (accessed 11th May 2024)

[8] G. W. C. Milner, E. Spivey, and J. W. Cobb, "155. The solid product of carbonisation," *Journal of the Chemical Society*, p. 578, Jan. 1943, doi: 10.1039/jr9430000578.

[9] F. Ronsse, S. Van Hecke, D. Dickinson, and W. Prins, "Production and characterization of slow pyrolysis biochar: influence of feedstock type and pyrolysis conditions," *Global Change Biology. Bioenergy/GCB Bioenergy*, vol. 5, no. 2, pp. 104–115, Oct. 2012, doi: 10.1111/gcbb.12018.

[10] X. Lu and X. Gu, "A review on lignin pyrolysis: pyrolytic behaviour, mechanism, and relevant upgrading for improving process efficiency," *Biotechnology for Biofuels and Bioproducts*, vol. 15, no. 1, Oct. 2022, doi: 10.1186/s13068-022-02203-0.

[11] S. R. Patlolla, K. Katsu, A. Sharafian, K. Wei, O. E. Herrera, and W. Mérida, "A review of methane pyrolysis technologies for hydrogen production," *Renewable & Sustainable Energy Reviews*, vol. 181, p. 113323, Jul. 2023, doi: 10.1016/j.rser.2023.113323.

[12] M. A. Martín-Lara, A. B. Pinar, A. Ligero, G. Blázquez, and M. Calero, "Characterization and Use of Char Produced from Pyrolysis of Post-Consumer Mixed Plastic Waste," *Water*, vol. 13, no. 9, p. 1188, Apr. 2021, doi: 10.3390/w13091188.

[13] M. Bernardo *et al.*, "Physico-chemical properties of chars obtained in the co-pyrolysis of waste mixtures," *Journal of Hazardous Materials*, vol. 219–220, pp. 196–202, Jun. 2012, doi: 10.1016/j.jhazmat.2012.03.077.

[14] S. E. Boslaugh, "Pyrolysis | Chemical reaction & energy conversion," *Encyclopedia Britannica*, May 30, 2014. https://www.britannica.com/science/pyrolysis

[15] "Topic: Global plastic waste," *Statista*, Jan. 10, 2024. https://www.statista.com/topics/5401/global-plastic-waste/#topicOverview

[16] B. Kwiecińska and H. I. Petersen, "Graphite, semi-graphite, natural coke, and natural char classification—ICCP system," *International Journal of Coal Geology*, vol. 57, no. 2, pp. 99–116, Feb. 2004, doi: 10.1016/j.coal.2003.09.003.

[17] J. Jagiełło, J. Judek, M. Zdrojek, M. Aksienionek, and L. Lipińska, "Production of graphene composite by direct graphite exfoliation with chitosan," *Materials Chemistry and Physics*, vol. 148, no. 3, pp. 507–511, Dec. 2014, doi: 10.1016/j.matchemphys.2014.09.043.

[18] S. M. Bulatovic "Beneficiation of graphite ore" *Handbook of Flotation Reagents: Chemistry, Theory and Practice; Amsterdam, The Netherlands: Elsevier* 2015, pp. 163-171.

[19] N. Vasumathi, T. V. Kumar, S. Ratchambigai, S. S. Rao, and G. B. Raju, "Flotation studies on low grade graphite ore from eastern India," *International Journal of Mining Science and Technology/International Journal of Mining Science and Technology*, vol. 25, no. 3, pp. 415–420, May 2015, doi: 10.1016/j.ijmst.2015.03.014.

[20] "Effect of Acid Leaching on Recovery of Graphite from Calcareous Deposits," *CORE Reader*, [Online]. Available: https://core.ac.uk/reader/297712260

[21] H. Ri *et al.*, "Effective purification of graphite via low pulp density flotation-low temperature alkali roasting-acid leaching route: From laboratory-scale to pilot-scale," *Minerals Engineering*, vol. 188, p. 107852, Oct. 2022, doi: 10.1016/j.mineng.2022.107852.

[22] W. J. Trahar, "A rational interpretation of the role of particle size in flotation," *International Journal of Mineral Processing*, vol. 8, no. 4, pp. 289–327, Oct. 1981, doi: 10.1016/0301-7516(81)90019-3.

[23] L. Wang, Y. Peng, K. Runge, and D. Bradshaw, "A review of entrainment: Mechanisms, contributing factors and modelling in flotation," *Minerals Engineering*, vol. 70, pp. 77–91, Jan. 2015, doi: 10.1016/j.mineng.2014.09.003.

[24] A. Vanderbruggen, A. M. Salces, A. Ferreira, M. Rudolph, and R. Serna-Guerrero, "Improving separation efficiency in End-of-Life Lithium-Ion batteries flotation using attrition Pre-Treatment," *Minerals*, vol. 12, no. 1, p. 72, Jan. 2022, doi: 10.3390/min12010072.

[25] H. Schubert, "On the optimization of hydrodynamics in fine particle flotation," *Minerals Engineering*, vol. 21, no. 12–14, pp. 930–936, Nov. 2008, doi: 10.1016/j.mineng.2008.02.012.

[26] R. Sivamohan, "The problem of recovering very fine particles in mineral processing — A review," *International Journal of Mineral Processing*, vol. 28, no. 3–4, pp. 247–288, May 1990, doi: 10.1016/0301-7516(90)90046-2.

[27] T. Miettinen, J. Ralston, and D. Fornasiero, "The limits of fine particle flotation," *Minerals Engineering*, vol. 23, no. 5, pp. 420–437, Apr. 2010, doi: 10.1016/j.mineng.2009.12.006.

[28] S. Arriagada, C. Acuña, and M. A. Vera, "New technology to improve the recovery of fine particles in froth flotation based on using hydrophobized glass bubbles," *Minerals Engineering*, vol. 156, p. 106364, Sep. 2020, doi: 10.1016/j.mineng.2020.106364.

[29] R. T. Rodrigues and J. Rubio, "DAF–dissolved air flotation: Potential applications in the mining and mineral processing industry," *International Journal of Mineral Processing*, vol. 82, no. 1, pp. 1–13, Feb. 2007, doi: 10.1016/j.minpro.2006.07.019.

[30] A. T. G. B. Hall and Dale, "Scaling up reuse and recycling of electric vehicle batteries: Assessing challenges and policy approaches," *Policy Commons*, Feb. 15, 2023. https://policycommons.net/artifacts/3809815/scaling-up-reuse-and-recycling-of-electric-vehicle-batteries/4615731/

[31] G. Manos, A. A. Garforth, and J. Dwyer, "Catalytic Degradation of High-Density Polyethylene over Different Zeolitic Structures," *Industrial & Engineering Chemistry Research*, vol. 39, no. 5, pp. 1198–1202, Mar. 2000, doi: 10.1021/ie990512q.

[32] G. Manos, A. A. Garforth, and J. Dwyer, "Catalytic degradation of High-Density polyethylene on an Ultrastable-Y zeolite. Nature of initial polymer reactions, pattern of formation of gas and liquid products, and temperature effects," *Industrial & Engineering Chemistry Research*, vol. 39, no. 5, pp. 1203–1208, Mar. 2000, doi: 10.1021/ie990513i.

[33] V. Dufaud and J. Basset, "Catalytic Hydrogenolysis at Low Temperature and Pressure of Polyethylene and Polypropylene to Diesels or Lower Alkanes by a Zirconium Hydride Supported on Silica-Alumina: A Step Toward Polyolefin Degradation by the Microscopic Reverse of Ziegler-Natta Polymerization," *Angewandte Chemie*, vol. 37, no. 6, pp. 806–810, Apr. 1998, doi: 10.1002/(sici)1521-3773(19980403)37:6.

[34] W. Kaminsky and I.-J. N. Zorriqueta, "Catalytical and thermal pyrolysis of polyolefins," *Journal of Analytical and Applied Pyrolysis*, vol. 79, no. 1–2, pp. 368–374, May 2007, doi: 10.1016/j.jaap.2006.11.005.

[35] İ. Çit, A. Sınağ, T. Yumak, S. Uçar, Z. Mısırlıoğlu, and M. Canel, "Comparative pyrolysis of polyolefins (PP and LDPE) and PET," *Polymer Bulletin*, vol. 64, no. 8, pp. 817–834, Dec. 2009, doi: 10.1007/s00289-009-0225-x.

[36] R. Aguado, M. Olazar, M. José, B. Gaisan, and J. Bilbao, "Wax formation in the pyrolysis of polyolefins in a conical spouted bed reactor," *Energy & Fuels*, vol. 16, no. 6, pp. 1429–1437, Sep. 2002, doi: 10.1021/ef020043w.

[37] N. Borsodi, A. Szentes, N. Miskolczi, C. Wu, and X. Liu, "Carbon nanotubes synthetized from gaseous products of waste polymer pyrolysis and their application," *Journal of Analytical and Applied Pyrolysis*, vol. 120, pp. 304–313, Jul. 2016, doi: 10.1016/j.jaap.2016.05.018.

[38] C. Quan, A. Li, and N. Gao, "Synthesis of carbon nanotubes and porous carbons from printed circuit board waste pyrolysis oil," *Journal of Hazardous Materials*, vol. 179, no. 1–3, pp. 911–917, Jul. 2010, doi: 10.1016/j.jhazmat.2010.03.092.

[39] M. A. Nahil, C. Wu, and P. T. Williams, "Influence of metal addition to Ni-based catalysts for the co-production of carbon nanotubes and hydrogen from the thermal processing of waste polypropylene," *Fuel Processing Technology*, vol. 130, pp. 46–53, Feb. 2015, doi: 10.1016/j.fuproc.2014.09.022.

[40] V. K. Bajpai and R. Singh, "Orthogonal Micro-Grooving of anisotropic pyrolytic carbon," *Materials and Manufacturing Processes*, vol. 26, no. 12, pp. 1481–1493, Dec. 2011, doi: 10.1080/10426914.2010.544811.

[41] U. Arena, M. L. Mastellone, G. Camino, and E. Boccaleri, "An innovative process for mass production of multi-wall carbon nanotubes by means of low-cost pyrolysis of polyolefins," *Polymer Degradation and Stability*, vol. 91, no. 4, pp. 763–768, Apr. 2006, doi: 10.1016/j.polymdegradstab.2005.05.029.

[42] "Polyethylene (PE plastic) – Structure, properties & toxicity." https://omnexus.specialchem.com/selection-guide/polyethylene-plastic

[43] "Reliance on Fossil Fuels Remains Virtually Unchanged Despite," January 4, 2024. https://www.fraserinstitute.org/article/reliance-on-fossil-fuels-remains-virtually-unchanged-despite-trillions-for-clean-energy .

[44] "Hydrogen production processes," *Energy.gov*. https://www.energy.gov/eere/fuelcells/hydrogen-production-processes (assessed 09-01-2024)

[45] "The hydrogen colour spectrum", https://www.nationalgrid.com/stories/energy-explained/hydrogen-colour-spectrum (assessed 09-01-2024)

[46] T. Keipi, K. Tolvanen, H. Tolvanen, and J. Konttinen, "Thermo-catalytic decomposition of methane: The effect of reaction parameters on process design and the utilization possibilities of the produced carbon," *Energy Conversion and Management*, vol. 126, pp. 923–934, Oct. 2016, doi: 10.1016/j.enconman.2016.08.060.

[47] T. Keipi, V. Hankalin, J. Nummelin, and R. Raiko, "Techno-economic analysis of four concepts for thermal decomposition of methane: Reduction of CO 2 emissions in natural gas combustion," *Energy Conversion and Management*, vol. 110, pp. 1–12, Feb. 2016, doi: 10.1016/j.enconman.2015.11.057.

[48] T. Keipi, T. Li, T. Løvås, H. Tolvanen, and J. Konttinen, "Methane thermal decomposition in regenerative heat exchanger reactor: Experimental and modeling study," *Energy*, vol. 135, pp. 823–832, Sep. 2017, doi: 10.1016/j.energy.2017.06.176.

[49] T. Keipi, H. Tolvanen, and J. Konttinen, "Economic analysis of hydrogen production by methane thermal decomposition: Comparison to competing technologies," *Energy Conversion and Management*, vol. 159, pp. 264–273, Mar. 2018, doi: 10.1016/j.enconman.2017.12.063.

[50] J. W. Beeckman and G. F. Froment, "Catalyst deactivation by active site coverage and pore blockage," *Industrial & Engineering Chemistry Fundamentals*, vol. 18, no. 3, pp. 245–256, Aug. 1979, doi: 10.1021/i160071a009.

[51] D. C. Upham *et al.*, "Catalytic molten metals for the direct conversion of methane to hydrogen and separable carbon," *Science*, vol. 358, no. 6365, pp. 917–921, Nov. 2017, doi: 10.1126/science.aao5023.

[52] G. Hartig, S. Gehringer, and H. Flachberger, "Preparation and refining of carbon pre-concentrates from pyrolysis processes into marketable carbon products with a view to large surfaces and high purities," *BHM. Berg- Und Hüttenmännische Monatshefte/Berg- Und Hüttenmännische Monatshefte*, vol. 166, no. 8, pp. 397–401, Aug. 2021, doi: 10.1007/s00501-021-01134-x.

[53] C. Engineering and C. Engineering, "Facts at your Fingertips: Agglomeration Processes," *Chemical Engineering*, Jan. 04, 2021. https://www.chemengonline.com/agglomeration-processes-2

[54] Wolfgang Pietsch: Agglomeration processes- Phenomena, Technologies, Equipment. Darmstadt, Germany: betz.druck GmbH ,2002. Wiley-VCH (2002) pg.133-134

[55] S. Jenkins, “Agglomeration processes,” *Document - Gale Academic OneFile*, Aug. 23, 2016. https://link.gale.com/apps/doc/A465466418/AONE?u=anon~6b787e1&sid=googleScholar&xid=49b6e1e5.

[56] K. V. S. Sastry and D. W. Fuerstenau, “Mechanisms of agglomerate growth in green pelletization,” *Powder Technology*, vol. 7, no. 2, pp. 97–105, Feb. 1973, doi: 10.1016/0032-5910(73)80012-9.

[57] Carlos Salas-Bringas1, Nevena Mišljenović2, Odd-Ivar Lekang1 and Reidar Barfod Schüller. Comparison between diametral and uniaxial compression tests of pelleted feed. ANNUAL TRANSACTIONS OF THE NORDIC RHEOLOGY SOCIETY, VOL. 19, 2011

[58] R. C. Brown, “The role of pyrolysis and gasification in a carbon negative economy,” *Processes*, vol. 9, no. 5, p. 882, May 2021, doi: 10.3390/pr9050882.

[59] F. Knabl, (2021). “*Structural Characterization of Carbons Derived from Methane Pyrolysis.”* [Master's Thesis, Montanuniversitaet Leoben (000)].

[60] G. I. Razd’yakonova, B. A. Лихолобов, L. V. Berezin, and O. A. Khamova, “New applications of carbon Black to increase the richness of soils,” *International Polymer Science and Technology*, vol. 41, no. 6, pp. 13–16, Jun. 2014, doi: 10.1177/0307174x1404100603.

[61] I. Santisteban *et al.*, “Loss on ignition: a qualitative or quantitative method for organic matter and carbonate mineral content in sediments,” *Journal of Paleolimnology*, vol. 32, no. 3, pp. 287–299, Oct. 2004, doi: 10.1023/b:jopl.0000042999.30131.5b.

[62] N. Chada, J. Romanos, R. Hilton, G. J. Suppes, J. Burress, and P. Pfeifer, “Activated carbon monoliths for methane storage,” *Bulletin of the American Physical Society*, vol. 2012, Mar. 2012, [Online]. Available: http://absimage.aps.org/image/MAR12/MWS_MAR12-2011-007660.pdf

[63] H. A. Pushpadass, A. Kumar, D. S. Jackson, R. L. Wehling, J. J. Dumais, and M. A. Hanna, "Macromolecular Changes in Extruded Starch-Films Plasticized with Glycerol, Water and Stearic Acid," *Stärke/Starch*, vol. 61, no. 5, pp. 256–266, May 2009, doi: 10.1002/star.200800046.

[64] L. C. F. Blackman, G. A. Saunders, and A. R. Ubbelohde, "Defect structure and properties of pyrolytic carbons," *Proceedings of the Royal Society of London. Series a, Mathematical and Physical Sciences*, vol. 264, no. 1316, pp. 19–40, Oct. 1961, doi: 10.1098/rspa.1961.0183.

[65] L. Zhang, R. Xu, H. Wang, Z. Wang, Y. Sun, and M. Li, "Chemical recycling of polyolefins: a closed-loop cycle of waste to olefins," *National Science Review/National Science Review*, vol. 10, no. 9, Aug. 2023, doi: 10.1093/nsr/nwad207.

[66] K. V. Khopade, S. H. Chikkali, and N. Barsu, "Metal-catalyzed plastic depolymerization," *Cell Reports Physical Science*, vol. 4, no. 5, p. 101341, May 2023, doi: 10.1016/j.xcrp.2023.101341.

[67] N. Singh, D. Hui, R. Singh, I. S. Ahuja, L. Feo, and F. Fraternali, "Recycling of plastic solid waste: A state of art review and future applications," *Composites. Part B, Engineering*, vol. 115, pp. 409–422, Apr. 2017, doi: 10.1016/j.compositesb.2016.09.013.

[68] H. Wang, Y. Zhang, and C. Wang, "Surface modification and selective flotation of waste plastics for effective recycling——a review," *Separation and Purification Technology*, vol. 226, pp. 75–94, Nov. 2019, doi: 10.1016/j.seppur.2019.05.052.

[69] Niu Xiaolu (2011) CN102504619B – "Purification process of pyrolysis carbon black of waste tire - Google Patents," Sep.29, 2011. https://patents.google.com/patent/CN102504619B/en

[70] "Will bubbles in the liquid affect Measurement of Magnetic Flow Meters?-Holykell-Measuring Instrument." https://www.holykell.com/Will-Bubbles-in-the-Liquid-Affect-Measurement-of-Magnetic-Flow-Meters.html

[71] M. Dworzanowski and Anglo American Technical Division, "Basic principles of magnetic separation," *The Journal of the Southern African Institute of Mining and Metallurgy*, vol. 110, p. 643, 2010, [Online]. Available: https://www.saimm.co.za/Journal/v110n11p643.pdf

[72] F. D. Öztürk and H. A. Temel, "Reverse flotation in Muş-Elmakaya Lignite beneficiation," *Energy Sources. Part a, Recovery, Utilization, and Environmental Effects*, vol. 35, no. 8, pp. 695–705, Apr. 2013, doi: 10.1080/15567036.2010.544009.

[73] H. Zhang, J. Liu, Y. Cao, and Y. Wang, "Effects of particle size on lignite reverse flotation kinetics in the presence of sodium chloride," *Powder Technology*, vol. 246, pp. 658–663, Sep. 2013, doi: 10.1016/j.powtec.2013.06.033.

[74] F. D. Öztürk, "Reverse flotation," in *InTech eBooks*, 2018. doi: 10.5772/intechopen.74082.

[75] J. Tan, L. Liang, Y. Peng, and G. Xie, "The concentrate ash content analysis of coal flotation based on froth images," *Minerals Engineering*, vol. 92, pp. 9–20, Jun. 2016, doi: 10.1016/j.mineng.2016.02.006.

[76] S. Farrokhpay, "The significance of froth stability in mineral flotation — A review," *Advances in Colloid and Interface Science*, vol. 166, no. 1–2, pp. 1–7, Aug. 2011, doi: 10.1016/j.cis.2011.03.001.

[77] B. A. Baitimbetova *et al.*, "Paramagnetic properties of carbon films," *Coatings*, vol. 13, no. 9, p. 1484, Aug. 2023, doi: 10.3390/coatings13091484.

[78] N. Rahimi *et al.*, "Solid carbon production and recovery from high temperature methane pyrolysis in bubble columns containing molten metals and molten salts," *Carbon*, vol. 151, pp. 181–191, Oct. 2019, doi: 10.1016/j.carbon.2019.05.041.

List of Abbreviations and Symbols

BF	Breakage Force
CMP	Carbon from methane plasmalysis
CS	Compressive Strength
CVD	Chemical Vapour Deposition
DE	Diatomaceous Earth
FC	Fixed carbon
LOI	Loss on Ignition
MSW	Municipal Solid Waste
MWCNT	Multiwalled Carbon Nano Tube
PET	Polyethylene Teraphthalate
PSD	Particle Size Distribution
PyCP	Pyrolytic Carbon from Polyolefins
SMR	Steam Methane Reforming
TDM	Thermal Decomposition of Methane
ρ ($\rho s, \rho f$)	Density (solid, fluid)
μ	Viscosity
g	Acceleration due to gravity
d	Diameter of particle
r	Radius of pellet
l	Length of pellet
V	Settling velocity
L/D	Length to Diameter of pellet

List of Tables

Table of Figures

Appendices

Appendix 1: Grade-recovery at 5 vol% graphite for different reagent

Appendix 1: Table of Grade recovery at 5vol% graphite

Denver cell	Mass	Mass	$m_{Loss(FC)}$ 1000°C 1h	Recovery	Cumm. Grade	Cumm. Rec.
	[g]	[%]	[%]	[%]	[%]	[%]
G.FLOT 1A FP1	85.5	59.6	95.1	63.0	95.0828434	63.0
G.FLOT 1A FP2	27.4	19.1	91.9	19.5	94.3207722	82.6
Reesidue	30.6	21.3	73.5	17.4	89.8857647	100.0
∑	143.4	100.0	89.9	100.0		

Denver cell	Mass	Mass	$m_{Loss(FC)}$ 1000°C 1h	Recovery	Cumm. Grade	Cumm. Rec.
	[g]	[%]	[%]	[%]	[%]	[%]
G.FLOT 1B FP1	93.6	64.4	95.0	67.7	95.03	67.65
G.FLOT 1B FP2	25.9	17.8	91.4	18.0	94.24	85.67
Reesidue	25.9	17.8	72.7	14.3	90.41	100.00
∑	145.4	100.0	90.4	100.0		

Denver cell	Mass	Mass	$m_{Loss(FC)}$ 1000°C 1h	Recovery	Cumm. Grade	Cumm. Rec.
	[g]	[%]	[%]	[%]	[%]	[%]
G.FLOT M FP1	70.0	48.7	93.8	51.0	93.81	51.00
G.FLOT M FP2	30.4	21.2	94.9	22.4	94.16	73.43
G.FLOT M FP3	18.1	12.6	92.5	13.0	93.91	86.46
Residue	25.2	17.5	69.1	13.5	89.57	100.00
∑	143.7	100.0	89.6	100.0		

Denver cell	Mass	Mass	$m_{Loss(FC)}$ 1000°C 1h	Recovery	Cumm. Grade	Cumm. Rec.
	[g]	[%]	[%]	[%]	[%]	[%]
G.FLOT DM FP1	69.4	47.2	93.1	49.0	93.06	48.98
G.FLOT DM FP2	41.4	28.1	94.0	29.5	93.42	78.45
G.FLOT DM FP3	20.1	13.6	91.4	13.9	93.10	92.36
Residue	16.3	11.1	61.8	7.6	89.63	100.00
∑	147.1	100.0	89.6	100.0		

Appendix 2: Grade and recovery for the different volume percent graphite using ekofol 452 reagent.

Appendix 2: Table of grade recovery for the different volume percent graphite

Denver cell	Mass [g]	Mass [%]	$m_{Loss(FC)}$ 1000°C 1h [%]	Recovery [%]	Cumm. Grade [%]	Cumm. Rec. [%]
G.FLOT 2 FP1	18.40	25.63	95.11	26.99	95.11	26.99
G.FLOT 2 FP2	24.18	33.69	97.03	36.19	96.20	63.18
G.FLOT 2 FP3	15.52	21.62	93.17	22.30	95.39	85.48
Residue	13.68	19.06	68.82	14.52	90.33	100.00
∑	71.78	100.00	90.33			

Denver cell	Mass [g]	Mass [%]	$m_{Loss(FC)}$ 1000°C 1h [%]	Recovery [%]	Cumm. Grade [%]	Cumm. Rec. [%]
G.FLOT 1 FP1	71.36	50.67	96.13	53.84	96.13	53.84
G.FLOT 1 FP2	25.11	17.83	94.14	18.55	95.61	72.39
G.FLOT 1 FP3	20.15	14.31	92.28	14.59	95.04	86.98
Residue	24.22	17.20	68.49	13.02	90.47	100.00
∑	140.84	100.00	90.47	100.00		

Denver cell	Mass [g]	Mass [%]	$m_{Loss(FC)}$ 1000°C 1h [%]	Recovery [%]	Cumm. Grade [%]	Cumm. Rec. [%]
G.FLOT 3 FP1	85.78	43.07	93.41	44.79	93.41	44.79
G.FLOT 3 FP2	41.54	20.86	94.40	21.92	93.73	66.71
G.FLOT 3 FP3	40.23	20.20	93.76	21.09	93.74	87.80
Residue	31.61	15.87	69.02	12.20	89.81	100.00
∑	199.16	100.00	89.81	100.00		

Denver cell	Mass [g]	Mass [%]	$m_{Loss(FC)}$ 1000°C 1h [%]	Recovery [%]	Cumm. Grade [%]	Cumm. Rec. [%]
G.FLOT 3ERR FI	115.00	57.70	93.41	60.00	93.41	60.00
G.FLOT 3ERR FI	49.10	24.64	93.13	25.54	93.33	85.55
Reesidue	35.20	17.66	73.51	14.45	89.83	100.00
∑	199.30	100.00	89.83	100.00		

Appendix 3: LOI of PyCP II flotation, reverse flotation, and magnetic products

Appendix 3: LOI for PyCP processes

LOI of PyCP Flotation Products for sample II

Sample	Products	crucible number	mass of cruc.(g	mass of cru. + sample before 1000°C (g)	Mass of sample(g	mass of cru. sample after 1000°C (g)	LOI (FC)c	ash (g)	%FC	%Ash
PFLOT	P1	13.2	15.32	15.90	0.57	15.56	0.34	0.23	59.30	40.70
		60	12.85	13.43	0.58	13.08	0.35	0.24	59.49	40.51
					1.15		**0.68**	0.47	**59.39**	40.61
	P2	7.1	12.71	13.21	0.50	12.92	0.29	0.20	58.90	41.10
		Y	12.55	13.01	0.46	12.74	0.27	0.19	58.88	41.12
					0.96		**0.56**	0.39	**58.89**	41.11
	P3	80	11.55	11.91	0.36	11.70	0.21	0.15	58.73	41.27
		6	12.09	12.56	0.47	12.28	0.28	0.19	58.84	41.16
					0.82		**0.48**	0.34	**58.79**	41.21
	Residue	5	12.83	13.38	0.55	13.04	0.34	0.20	62.92	37.08
		1.1	12.83	13.41	0.58	13.05	0.36	0.22	62.80	37.20
					1.12		**0.71**	0.42	**62.86**	37.14
				REVERSE FLOTATION						
RFLOT	P1	19	12.73	13.18	0.45	12.92	0.26	0.19	58.46	41.54
		X	11.81	12.31	0.49	12.02	0.29	0.20	58.48	41.52
					0.94		**0.55**	0.39	**58.47**	41.53
	P2	32	12.60	13.11	0.51	12.81	0.30	0.21	58.53	41.47
		14	11.87	12.34	0.47	12.06	0.28	0.20	58.63	41.37
					0.98		**0.58**	0.41	**58.57**	41.43
	P3	200	10.55	11.05	0.50	10.76	0.29	0.21	58.43	41.57
		46	13.36	13.81	0.45	13.55	0.26	0.19	58.38	41.62
					0.95		**0.56**	0.40	**58.40**	41.60
	P4	2.1	12.88	13.37	0.49	13.08	0.29	0.20	59.06	40.94
		44	12.61	13.13	0.53	12.82	0.31	0.21	59.12	40.88
					1.01		**0.60**	0.41	**59.10**	40.90
	Residue	3	14.98	15.44	0.46	15.13	0.31	0.15	67.10	32.90
		4.1	12.55	13.12	0.57	12.74	0.37	0.19	66.30	33.70
					1.03		**0.68**	0.34	**66.66**	33.34
				MAGNETIC SEPARATION						
MAG	P1	3.1	12.84	13.41	0.57	13.07	0.34	0.23	59.55	40.45
		3.3	12.60	13.08	0.49	12.79	0.29	0.20	59.59	40.41
					1.05		**0.63**	0.43	**59.57**	40.43
NMAG	P2	2.2	12.33	12.81	0.48	12.53	0.29	0.19	59.65	40.35
		45	12.53	12.95	0.42	12.70	0.25	0.17	59.65	40.35
					0.90		**0.54**	0.36	**59.65**	40.35

Appendix 4: Individual BF trials for granules of 3 wt% lignosulfonate binder

Appendix 4: BF of granules for 3% lignosulfonate

size(mm)	# S/N	A	# S/N	B	# S/N	C	# S/N	D	# S/N	E	# S/N	F	# S/N	G
5	165	0.3	103	8							155	1.335	92	1.2
	167	0.545	104	13.18							156	0.9	93	1.065
	169	0.41	106	14							157	0.71	94	1.09
	170	0.275	107	20.55							158	0.795	95	1.035
	171	0.41	108	11.08							159	1.145	96	0.68
	AVERAGE	**0.388**		**13.362**								**0.977**		**1.014**
4	160	0.685	98	8	121	3.385	131	1.535			144	0.955	82	0.985
	161	0.545	99	6.685	124	3.55	132	1.175			145	0.57	83	0.6
	162	0.465	100	5.515	125	3.71	133	1.775			146	0.955	84	0.515
	163	0.515	101	3.465	122	2.62	134	2.32			147	0.71	85	0.955
	164	0.545	102	6.5	123	4.72	135	1.12			148	0.74	86	0.76
		0.551		**6.033**		**3.597**		**1.585**				**0.786**		**0.763**
3.15	172	0.215	109	10.15	115	1.965	126	0.82	137	0.52	149	0.545	87	0.41
	173	0.444	110	4.065	117	2.075	127	1.04	138	0.435	151	0.4	88	0.63
	174	0.41	111	2.51	118	2.078	128	0.85	140	0.44	152	0.655	89	0.845
	175	0.6	112	5.35	119	2.175	129	1.585	141	0.435	153	0.655	90	0.795
	176	0.49	113	3.845	120	3.14	130	1.09	142	0.465	154	0.71	91	0.6
		0.4318		**5.184**		**2.2866**		**1.077**		**0.459**		**0.593**		**0.656**

Appendix 5: Trials for BF of pellets with varying moisture content using 3% lignosulfonate binder.

Appendix 5: BF of pellets for 3% lignosulfonate

Refrence for CF	23	N	Pelletizing forc	3500	N
diameter of pellet	2	cm	Pelletizing pressur	11140846	N/m2
depth of die	7.5	cm	Pelletizing pres	11.14085	Mpa
dislacment rate	10	mm/min			

wt% of water	Trials	Pressure agglomeration measurements displacement(mm)	time(secs)	weight before drying(g) bowl	bowl+sample	sample	weight after drying(g) bowl+sample	sample	mass of water	% mass of water	BF(N)	Length of press(cm) L (cm)	L/D
5%	a	29	174	140.54	144.45	3.91	144.4	3.86	0.05	1.28	8.61	1.5	
	b	34	204	131.26	135.83	4.57	135.78	4.52	0.05	1.09	10.39	1.8	
	c	31	186	139.22	143.03	3.81	143.01	3.79	0.02	0.52	7.49	1.3	
	Average	**31.33**	**188**			**4.10**		**4.06**	**0.04**	**0.97**	**8.83**	**1.53**	**0.77**
10%	a	39	234	138.75	142.23	3.48	142.21	3.46	0.02	0.57	12	1.4	
	b	41	246	132.15	136.73	4.58	136.7	4.55	0.03	0.66	8.8	1.7	
	c	35	210	141.14	146.89	5.75	146.87	5.73	0.02	0.35	38.26	**1.6**	
	Average	**38.33**	**230**			**4.60**		**4.58**	**0.02**	**0.53**	**19.69**	**1.57**	**0.78**
15%	a	30	180	138.74	146.12	7.38	144.94	6.2	1.18	15.99	38.64	2.2	
	b	33	198	139.46	147.1	7.64	145.91	6.45	1.19	15.58	50.68	2.5	
	c	26	156	146.37	153.67	7.3	152.53	6.16	1.14	15.62	53.93	2.4	
	Average	**29.67**	**178**			**7.44**		**6.27**	**1.17**	**15.73**	**47.75**	**2.37**	**1.18**
20%	a	31	186	152.02	161.32	9.3	159.32	7.3	2	21.51	69.48	2.6	
	b	37	222	131.29	139.97	8.68	138.18	6.89	1.79	20.62	61.68	2.6	
	c	26	156	135.23	144.46	9.23	142.56	7.33	1.9	20.59	65.39	2.6	
	Average	**31.33**	**188**			**9.07**		**7.17**	**1.90**	**20.90**	**65.52**	**2.60**	**1.30**
25%	a	26	156	140.53	149.14	8.61	146.99	6.46	2.15	24.97	58.13	2.5	
	b	32	192	141.55	150.08	8.53	148.02	6.47	2.06	24.15	61.41	2.5	
	c	30	180	151.33	160.21	8.88	158.02	6.69	2.19	24.66	75.32	2.5	
	Average	**29.33**	**176**			**8.67**		**6.54**	**2.13**	**24.59**	**64.95**	**2.50**	**1.25**
30%	a	29	174	142.58	153.36	10.78	150.22	7.64	3.14	29.13	52.72	2.8	
	b	26	156	140.16	151.57	11.41	148.24	8.08	3.33	29.18	52.67	3	
	c	29	174	130.74	141.92	11.18	138.69	7.95	3.23	28.89	63.07	3	
	Average	**28.00**	**168**			**11.12**		**7.89**	**3.23**	**29.07**	**56.15**	**2.93**	**1.47**
35%	a	22	132	139.95	154.15	14.2	149.41	9.46	4.74	33.38	79.8	3.8	
	b	24	144	205.93	220.22	14.29	215.44	9.51	4.78	33.45	71.06	3.7	
	c	24	144	139.69	154.32	14.63	149.43	9.74	4.89	33.42	44.13	3.6	
	Average	**23.33**	**140**			**14.37**		**9.57**	**4.80**	**33.42**	**65.00**	**3.70**	**1.85**
40%	a®	21	126	132.23	148.59	16.36	143.18	10.95	5.41	33.07	31.91	3.5	
	b(d)	18	108	142.72	155.85	13.13	151.57	8.85	4.28	32.60	33.14	4.5	
	c(g)	21	126	140.27	150.21	9.94	147.05	6.78	3.16	31.79	18.54	2.5	
	Average	**20.00**	**120**			**13.14**		**8.86**	**4.28**	**32.49**	**27.86**	**3.50**	**1.75**

Appendix 6: BF for Pellets using DE binder with constant moisture content.

Appendix 6: BF for pellets for DE binder

					diameter of pellet			2 cm		Pelletizing force		3500 N
					depth of die			7.5 cm		Pelletizing pressure		792237.9389 N/m2
					dislacment rate			10 mm/min		Pelletizing pressure		0.792237939 Mpa
wt% of water	Trials	weight before drying(g)			weight after drying(g)		%	BF(N)		Length of press(cm)		
		bowl	bowl+sample	sample	bowl+sam	sample	mass of wate	mass of water		L/D		
8.7%	a	135.30	142.21	6.91	140.72	5.42	1.49	21.56		2.00		
	b	140.60	147.59	6.99	146.02	5.42	1.57	22.46		2.00		
	c	131.10	137.98	6.88	136.52	5.42	1.46	21.22		2.00		
	Average			**6.93**		**5.42**	**1.51**	**21.75**		**2.00**	**1.00**	
15%	a	141.61	151.03	9.42	148.53	6.92	2.50	26.54	23.90	2.80		
	b	140.00	149.86	9.86	147.22	7.22	2.64	26.77	20.58	2.80		
	c	140.33	150.32	9.99	147.57	7.24	2.75	27.53	18.56	2.80		
	Average			**9.76**		**7.13**	**2.63**	**26.95**	**21.01**	**2.80**	**1.40**	
20%	a	142.80	153.66	10.86	150.44	7.64	3.22	29.65	30.33	3.00		
	b	139.51	151.08	11.57	147.57	8.06	3.51	30.34	32.50	3.00		
	c	138.79	150.40	11.61	146.84	8.05	3.56	30.66	26.48	3.00		
	Average			**11.35**		**7.92**	**3.43**	**30.22**	**29.77**	**3.00**	**1.50**	
8.7% +10%CLAY	a	152.09	160.10	8.01	158.54	6.45	1.56	19.48		2.60		
	b	146.42	153.86	7.44	152.41	5.99	1.45	19.49		2.60		
	c	131.34	139.39	8.05	137.80	6.46	1.59	19.75	0.50	2.60		
	Average			**7.83**		**6.30**	**1.53**	**19.57**	**0.50**	**2.60**	**1.30**	